WARWICK

Library Declaration and Deposit Agreement

1. STUDENT DETAILS

Please complete the following:

Full name: MARK SKELTON

University ID number: 1308812

2. THESIS DEPOSIT

2.1 Under your registration at the University, you are required to deposit your thesis with the University in BOTH hard copy and in digital format. The digital copy should normally be saved as a single pdf file.

2.2 The hard copy will be housed in the University Library. The digital copy will be deposited in the University's Institutional Repository (WRAP). Unless otherwise indicated (see 2.6 below), this will be made immediately openly accessible on the Internet and will be supplied to the British Library to be made available online via its Electronic Theses Online Service (EThOS) service.
[At present, theses submitted for a Master's degree by Research (MA, MSc, LLM, MS or MMedSci) are not being deposited in WRAP and not being made available via EthOS. This may change in future.]

2.3 In exceptional circumstances, the Chair of the Board of Graduate Studies may grant permission for an embargo to be placed on public access to the thesis **in excess of two years**. This must be applied for when submitting the thesis for examination (further information is available in the *Guide to Examinations for Higher Degrees by Research.*)

2.4 If you are depositing a thesis for a Master's degree by Research, the options below only relate to the hard copy thesis.

2.5 If your thesis contains material protected by third party copyright, you should consult with your department, and if appropriate, deposit an abridged hard and/or digital copy thesis.

2.6 Please tick one of the following options for the availability of your thesis (guidance is available in the *Guide to Examinations for Higher Degrees by Research)*:

☑ Both the hard and digital copy thesis can be made publicly available immediately

☐ The hard copy thesis can be made publicly available immediately and the digital copy thesis can be made publicly available after a period of two years (*should you subsequently wish to reduce the embargo period please inform the Library*)

☐ Both the hard and digital copy thesis can be made publicly available after a period of two years (*should you subsequently wish to reduce the embargo period please inform the Library*)

☐ Both the hard copy and digital copy thesis can be made publicly available after _____ (insert time period in excess of two years). **This option requires the prior approval of the Chair of the Board of Graduate Studies (see 2.3 above)**

2.7 The University encourages users of the Library to utilise theses as much as possible, and unless indicated below users will be able to photocopy your thesis.

☐ I **do not** wish for my thesis to be photocopied

3. GRANTING OF NON-EXCLUSIVE RIGHTS

Whether I deposit my Work personally or through an assistant or other agent, I agree to the following:

- Rights granted to the University of Warwick and the British Library and the user of the thesis through this agreement are non-exclusive. I retain all rights in the thesis in its present version or future versions. I agree that the institutional repository administrators and the British Library or their agents may, without changing content, digitise and migrate the thesis to any medium or format for the purpose of future preservation and accessibility.

4. DECLARATIONS

I DECLARE THAT:

- I am the author and owner of the copyright in the thesis and/or I have the authority of the authors and owners of the copyright in the thesis to make this agreement. Reproduction of any part of this thesis for teaching or in academic or other forms of publication is subject to the normal limitations on the use of copyrighted materials and to the proper and full acknowledgement of its source.

- The digital version of the thesis I am supplying is either the same version as the final, hard-bound copy submitted in completion of my degree once any minor corrections have been completed, or is an abridged version (see 2.5 above).

- I have exercised reasonable care to ensure that the thesis is original, and does not to the best of my knowledge break any UK law or other Intellectual Property Right, or contain any confidential material.

- I understand that, through the medium of the Internet, files will be available to automated agents, and may be searched and copied by, for example, text mining and plagiarism detection software.

- At such time that my thesis will be made publically available digitally (see 2.6 above), I grant the University of Warwick and the British Library a licence to make available on the Internet the thesis in digitised format through the Institutional Repository and through the British Library via the EThOS service.

- If my thesis does include any substantial subsidiary material owned by third-party copyright holders, I have sought and obtained permission to include it in any version of my thesis available in digital format and that this permission encompasses the rights that I have granted to the University of Warwick and to the British Library.

5. LEGAL INFRINGEMENTS

I understand that neither the University of Warwick nor the British Library have any obligation to take legal action on behalf of myself, or other rights holders, in the event of infringement of intellectual property rights, breach of contract or of any other right, in the thesis.

Please sign this agreement and ensure it is bound into the final hard bound copy of your thesis, which should be submitted to Student Reception, Senate House.

Student's signature: M.S.Kelton Date: 8th May 2018

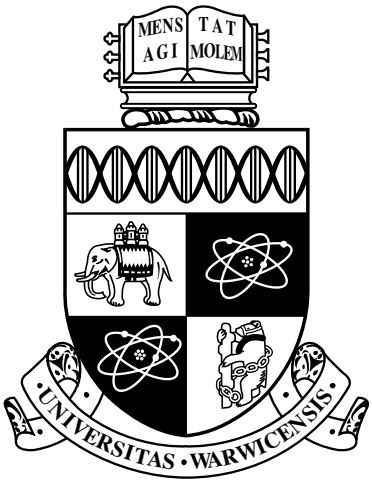

How Does a Bohm Particle Localize?

by

Mark Skelton

Thesis

Submitted to the University of Warwick

for the degree of

Master of Science by Research

Department of Physics

January 2018

THE UNIVERSITY OF
WARWICK

Contents

List of Figures

List of Tables

Acknowledgments

I would like to thank Professor Rudolf Roemer and Edoardo Carnio who have regularly asked for updates to the project which has kept me motivated, and for their guidance and insight throughout the project.

Also many thanks to all the physics postgraduate students for their general advice, support and friendship. I must also thank my close friends who helped me get through this project; their companionship has helped me get through the more difficult moments.

I would like to thank my family for their help emotionally, and for getting me through the thesis writing stage.

Lastly, I would like to thank anyone else who helped me that I could have forgotten to mention here.

Declarations

I declare that the research presented in this thesis is my own work and that I have correctly acknowledged the work of others. This thesis is in accordance with University guidance on good academic conduct, including guidance on how to avoid plagiarism and advice for referencing sources, available at: https://warwick.ac.uk/services/ library/students/referencing/

I also declare that this thesis has not been submitted for a degree at another university, only to the University of Warwick.

Abstract

Using de-Broglie Bohm theory, an interpretation of quantum mechanics with deterministic particle trajectories, instead of the usual Copenhagen interpretation, where properties of particles only exist upon measurement, can be useful in studying a system in terms of non-linear dynamics. Specifically it is possible to measure the Lyapunov exponents of Bohm trajectories, so in this project de Broglie-Bohm theory is applied in the context of Anderson localization in one-dimension by utilizing a computer simulation to evolve the system and to track the trajectories of the Bohm particles. By studying the trajectories using time series analysis the Anderson model can be studied in a unique way, producing results which can also be shown by the usual methods and opening the door to research not possible in the Copenhagen interpretation. The average maximal Lyapunov exponent over many realisations of the system is found for each trajectory and plotted as a function of trajectory initial position. These plots are produced for each value of disorder which show peaks of average maximal Lyapunov exponent, where Gaussian curves are fitted and the root mean square width is measured. These widths show a potential quadratic relation to disorder, so by using the Thouless formula the localization length can be found purely by looking at the dynamics of the trajectories. By plotting the distribution of maximal Lyapunov exponents per trajectory, individual trajectories could be analysed though further work is required to find out how. Another route for studying the trajectories involves plotting histograms of their final positions, and also the average velocities per trajectory over the simulation time, which can be used to show whether the system is in the localized or diffusive state.

Abbreviations

deBB	de Broglie-Bohm	1
FFT	fast Fourier transform	14
MLE	maximal Lyapunov exponent	10
RMS	root mean square	7

Chapter 1

Introduction

In attempting to unify quantum physics with general relativity and gravity, some have posited (Hardy and Spekkens [2010]) that the reason that it has not been accomplished is due to an incomplete description of the current quantum theory. The interpretations of quantum mechanics attempt to give more meaning to the definition of the wave function and explain a process for the wave function collapse upon measurement. There are many different interpretations of quantum mechanics such as the Many Worlds Interpretation (Everett [1956]), the Transactional Interpretation (Cramer [2015]), Decoherent Histories (Gell Mann and B. Hartle [2011]), Quantum Darwinism (Zurek [2009]), and the Cosmological Interpretation (Aguirre and Tegmark [2011]). The interpretation of interest in this project is the de Broglie-Bohm (deBB) theory (Bohm [1952a] and Bohm [1952b]). In order to define the wave function more completely, deBB theory makes a return to determinism. The quantum probability in this theory originates simply from our lack of knowledge of the initial conditions, and a given particle has definite properties regardless of whether a measurement is taking place or not. However it is worth noting that, just like in ordinary quantum theory, deBB theory does not yet explain why the probability distribution is as described in the Born probability rule (Holland [1995]), although there are suggestions that it arises naturally from the particle dynamics of deBB theory. In Towler et al. [2012] and Valentini and Westman [2005] numerical calculations are conducted where the initial probability distribution is not that given by the Born rule. After evolving the system for a certain number of time steps the probability distribution converges towards the Born rule, showing that the Born rule may not need to be considered as an axiom in this interpretation but could later be shown to be an emerging feature.

As stated in the first of the original pair of articles for deBB theory (Bohm

[1952a]), the theory gives a more general mathematical formalism than the usual Copenhagen interpretation that could show what occurs at distances of the order 10^{-13} cm or less, allowing physical phenomena at these very small distances to be described. The second article (Bohm [1952b]) proves that any predictions made about the results of measurements in deBB theory match those of the Copenhagen interpretation, with the uncertainty principle being a practical limitation in deBB theory compared to it being inherent in the Copenhagen interpretation. The uncertainty is said to arise from unpredictable disturbances of the observed system by the measuring apparatus.

In deBB theory a particle is guided by a wave, described by the wave function, that has some physical manifestation in real space. The gradient of the phase, with respect to position, provides the velocity field used to describe particle motion. Nodal regions of the wave function are points in space where the amplitude of the wave is zero, and so the particle can never enter these regions. Frisk [1997] shows that if the wave function has many nodes then the trajectories are chaotic. It has also been proven that the motion of vortices in the associated velocity field can lead to chaotic behaviour of the trajectories (Borondo et al. [2009]). Indeed in deBB theory it is possible to have a strong definition of a chaotic system due to particles travelling in classical-like trajectories, therefore the Lyapunov exponents of these trajectories can be found. In contrast, for the Copenhagen interpretation a definition of chaos is much less clear since it does not make sense to consider the position of a particle in between measurements. Using deBB theory, quantum systems such as the quantum kicked rotator and a two-dimensional anisotropic oscillator have been studied using chaos theory (Iacomelli and Pettini [1996]). As for one-dimensional quantum systems, de Alcantara Bonfim et al. [1998] found chaotic behaviour in one dimension for a single particle in a double square-well potential, which is a square barrier embedded in an infinite well. This goes against claims that chaotic behaviour in one-dimensional quantum systems is impossible, with Parmenter and Valentine [1995] stating that at least two degrees of freedom are required for the system to show chaos. Yang and Wei [2008] suggests that since there exists no evidence showing significant reduction in the trajectory complexity for one-dimensional systems the possibility of finding chaos in one-dimensional systems cannot be rejected. Yang and Wei [2008] then showed that chaos does indeed exist in one-dimensional quantum systems if the domain for the trajectories is extended to the complex plane by characterising the quantum world by a four-dimensional complex spacetime using the $E^{(\infty)}$ theory.

In this project a closer look at Anderson localization (Anderson [1958]) is taken using deBB theory. The study is conducted using a numerical simulation of

the system, with the output trajectories treated as a time series for analysis. The trajectories are propagated in real space, so normal analysis of the trajectories by considering their Lyapunov exponents is conducted to observe if any chaotic behaviour exists. The results show that the trajectories exhibit some chaotic behaviour in this system, with maximal Lyapunov exponents of the order 10^{-3} or less relative to the units of time used in the code, which leads to an alternative way of studying the Anderson model compared to the Copenhagen interpretation. More specifically one can determine properties of the system, such as the localization length and whether the system is in the localized or diffusive state, purely using the trajectories of the Bohm particles. Also individual trajectories can be analysed so that phenomena at lengths scales smaller than that possible in the usual quantum theory could be described. However further work is required to determine the nature of such phenomena.

Chapter 2

Literature Review

The following chapter includes all the relevant background material that is needed for the simulation and for analysing its output. A brief derivation of the equations of motion for the trajectories in deBB theory is given, along with the solution to the equation of motion of a Bohm particle guided by a free Gaussian wave packet in one dimension. Some theory on Anderson localization and localization length is given, including the Thouless formula, and finally concepts and definitions for chaos theory are outlined.

2.1 de Broglie-Bohm Theory

The meaning of the wave function according to deBB theory is for it to be a physically real part of the system. Consider a single particle system; then the wave described by the wave function is said to guide the particle, exerting a force on it such that repeated experiments reproduce the results of the usual quantum theory. The quantum probability arises simply from our lack of knowledge of the initial conditions, and a given particle has a deterministic trajectory regardless of any measurement occurring. Therefore there is no wave function collapse upon measurement (Holland [1995]). The equations of motion for the particle are derived directly using the Schrödinger equation, and this derivation is shown here before an example solution is given.

2.1.1 Derivation and General Ideas

Let $\psi(\boldsymbol{x}, t)$ be a wave function, at position $\boldsymbol{x}$ and time t, of the form

$$\psi(\boldsymbol{x}, t) = R(\boldsymbol{x}, t) \exp\left(\frac{iS(\boldsymbol{x}, t)}{\hbar}\right) \tag{2.1}$$

with $R(\boldsymbol{x},t)$ representing the amplitude, $S(\boldsymbol{x},t)$ the phase and $\hbar$ the reduced Planck constant. Substituting $\psi(\boldsymbol{x},t)$ into the time dependent Schrödinger equation

$$i\hbar\frac{\partial}{\partial t}\psi(\boldsymbol{x},t) = \left(\frac{-\hbar^2}{2m}\nabla^2 + V(\boldsymbol{x},t)\right)\psi(\boldsymbol{x},t), \tag{2.2}$$

where m is the mass of the particle and $V(\boldsymbol{x},t)$ is the potential, and then equalling real and imaginary parts gives

$$\frac{\partial S}{\partial t} + \frac{(\nabla S)^2}{2m} + Q + V = 0, \tag{2.3a}$$

$$\frac{\partial R^2}{\partial t} + \nabla\cdot\left(\frac{R^2\nabla S}{m}\right) = 0, \tag{2.3b}$$

with

$$Q(\boldsymbol{x},t) = -\frac{\hbar^2}{2m}\frac{\nabla^2 R}{R} \tag{2.4}$$

representing the quantum potential. In deBB theory ψ is treated as a physical wave propagating in space with a point particle of mass m which follows a trajectory $\boldsymbol{x} = \boldsymbol{x}(t)$. This wave and particle pair are treated as a single physical system, with the wave exerting a force on the particle. Note that the particle does not interact with the wave, which is an example of a non-classical property of the theory (Holland [1995]).

The connection between particle and wave is given by equation (2.3a) which is a generalized form of the Hamilton-Jacobi equation (Holland [1995]), with the total potential being $Q(\boldsymbol{x},t) + V(\boldsymbol{x},t)$. So $V(\boldsymbol{x},t)$ is regarded as the classical potential and $Q(\boldsymbol{x},t)$ is the quantum potential (Bohm [1952a]).

Using ordinary Hamilton-Jacobi theory (Uppu [2007]), a velocity field is determined from the solution to equation (2.3a)

$$\boldsymbol{v}(\boldsymbol{x},t) = \frac{\nabla S(\boldsymbol{x},t)}{m} \tag{2.5}$$

From equation (2.3a) a form of Newton's second law can be derived with force $-\nabla(V+Q)$ which shows that it is appropriate to consider Q as a potential in the same regard as V with respect to particle motion. To do this the operator ∇ is applied to equation (2.3a) which after some rearranging yields

$$\left[\frac{\partial}{\partial t} + \frac{1}{m}\nabla S\cdot\nabla\right]\nabla S = -\nabla(V+Q). \tag{2.6}$$

Then, using the equation of motion (2.5), the equation (2.6) can be simplified to

$$\frac{d}{dt}(m\dot{\boldsymbol{x}}) = -\nabla(V+Q)|_{\boldsymbol{x}=\boldsymbol{x}(t)} \tag{2.7}$$

with

$$\frac{d}{dt} = \frac{\partial}{\partial t} + \dot{\boldsymbol{x}} \cdot \nabla. \tag{2.8}$$

Equation (2.7), which can also be considered a particle law of motion, shows a form of Newtons second law with the additional quantum potential ∇Q on top of the usual classical potential ∇V.

In order to find the trajectory that a particle takes the only initial conditions required are the initial position $\boldsymbol{x}_0$, the initial wave function ψ_0 and the potential V. Note that the initial velocity of the particle does not need to be stated since it is uniquely given by the equation of motion (2.5) using ψ_0. With these initial conditions it is possible to track the particle trajectory for all time afterwards. This could be done by solving the Schrödinger equation for the wave function and then solving the equation of motion (2.5) for the particle trajectory (Holland [1995]).

In practice it is not possible to know the initial conditions of the system precisely, due to unpredictable and uncontrollable perturbations of the system by the measuring apparatus (Bohm [1952b]), and so a range of values for $\boldsymbol{x}_0$ and ψ_0 are considered which produces an ensemble of non-interacting systems.

Assuming maximal knowledge of the initial wave, so that ψ_0 is fixed, means that in a sequence of trials only $\boldsymbol{x}_0$ varies, which is distributed according to $\rho_0(\boldsymbol{x})$. In order for this distribution to be the one given by the Born rule, first assume R_0^2 is normalizable

$$\int R_0^2(\boldsymbol{x}) d^3x = 1. \tag{2.9}$$

Then it is sufficient to postulate that

$$\rho_0(\boldsymbol{x}) = R_0^2(\boldsymbol{x}). \tag{2.10}$$

Since $R^2(\boldsymbol{x},t)$ satisfies equation (2.3b), which is the equation of continuity from Hamilton-Jacobi theory

$$\frac{\partial \rho}{\partial t} + \nabla \cdot (\rho \boldsymbol{v}) = 0, \tag{2.11}$$

then $R^2(\boldsymbol{x},t)$ determines the probability distribution for all time t if the above postulate holds. That is, $\rho(\boldsymbol{x},t) = R^2(\boldsymbol{x},t)$ and R^2 is normalized for all t. Note that

there is no real reason for this postulate to be true apart from the fact that it follows the quantum theory (Holland [1995]), though Towler et al. [2012] and Valentini and Westman [2005] show that it likely emerges from the particle dynamics by using computer simulations.

Some final observations follow. The trajectories of these particles cannot cross since then the value of $\nabla S(\boldsymbol{x}, t)$ would take on two different values at the same point $(\boldsymbol{x}, t)$. Additionally, they obviously cannot enter nodal regions, where $R(\boldsymbol{x}, t) = 0$.

So to summarise, the wave and particle are considered to be a single system with the wave, described by equation (2.1), evolving via equation (2.2) and interacting with the particle via equation (2.3a). Also, the probability arises from our lack of knowledge of the initial system and not from some intrinsic probability. From Hamilton-Jacobi theory, the equation of motion of the particle is given by equation (2.5) (Holland [1995]).

2.1.2 Free Gaussian Packet

The initial form of a one-dimensional Gaussian wave packet at each position x is

$$\psi_0(x) = \frac{1}{(2\pi\sigma_0^2)^{1/4}} \exp\left(ikx - \frac{x^2}{4\sigma_0^2}\right), \tag{2.12}$$

where σ_0 is the root mean square (RMS) width of the wave and k is the wavenumber. Since the expectation value of the momentum operator is given as $\langle\hat{p}\rangle = \hbar k$, the centre of the wave packet initially has group velocity $u = \hbar k/m$, where as usual $\hbar$ represents the reduced Planck constant and m the mass of the particle. The free Schrödinger evolution of this Gaussian wave packet gives the equation of the wave at any time t,

$$\psi(x, t) = \frac{1}{(2\pi s_t^2)^{1/4}} \exp\left(ik\left(x - \frac{1}{2}ut\right) - \frac{(x - ut)^2}{4s_t\sigma_0}\right), \tag{2.13}$$

with

$$s_t = \sigma_0\left(1 + \frac{i\hbar t}{2m\sigma_0^2}\right) \tag{2.14}$$

This yields the amplitude R and phase S functions,

$$R(x,t) = \frac{1}{(2\pi\sigma^2)^{1/4}} \exp\left(\frac{-(x-ut)^2}{4\sigma^2}\right), \tag{2.15a}$$

$$S(x,t) = -\frac{3\hbar}{2}\arctan\left(\frac{\hbar t}{2m\sigma_0^2}\right) + mu\left(x - \frac{1}{2}ut\right) + \frac{(x-ut)^2\hbar^2 t}{8m\sigma_0^2\sigma^2}, \tag{2.15b}$$

with σ being the RMS width of the wave at a given time t, with its value given by the modulus of the complex number s_t,

$$\sigma = |s_t| = \sigma_0\left[1 + \left(\frac{\hbar t}{2m\sigma_0^2}\right)^2\right]^{1/2} \tag{2.16}$$

The mean position $\langle x\rangle$ can be calculated using the definition for the expectation value of $\hat{x}$,

$$\langle\hat{x}\rangle = \int_{-\infty}^{\infty} x|\psi(x,t)|^2 dx, \tag{2.17}$$

which gives $\langle x\rangle = ut$. So the mean average position moves as a (classical) free particle, with

$$\langle x\rangle = \frac{\hbar k t}{m}. \tag{2.18}$$

Differentiate $S(x,t)$ with respect to x to get

$$\nabla S = mu + \frac{(x-ut)\hbar^2 t}{4m\sigma_0^2\sigma^2}. \tag{2.19}$$

Using $v = \nabla S/m$ with equation (2.19) then gives the velocity field as

$$v = u + \frac{(x-ut)\hbar^2 t}{4m^2\sigma_0^2\sigma^2}. \tag{2.20}$$

We note that no matter what the starting position is, the initial velocity of the particle is always u. Finally, by solving equation (2.20) as a first order linear differential equation, the equation for the particle trajectory is found to be

$$x(t) = ut + x_0\left[1 + \left(\frac{\hbar t}{2m\sigma_0^2}\right)^2\right]^{1/2}, \tag{2.21}$$

with x_0 the initial position. This equation can be interpreted by splitting the right hand side into two parts, with the first part reflecting the overall motion of the wave and the second term originating from the spreading of the wave. If the initial

position $x_0 = 0$, so the particle starts at the centre of the wave, then the particle stays there and moves uniformly as a classically free particle for all time t afterwards. Additionally, suppose the wave has group velocity $u = 0$, and $x = \sigma(t)$ represents the motion of a point in the packet initially at $x = \sigma_0$. Then a particle initially at $x_0 = \sigma_0$ has the same motion as the aforementioned point in the wave initially at $x = \sigma_0$, seen by simply comparing equations (2.21) and (2.16) (Holland [1995]).

2.2 Anderson Localization

It is claimed (Bohm [1952b]) that deBB theory reproduces the experimental results predicted by quantum mechanics with certainty. Even so there are many contexts that it has not yet been realised in. One such context that has yet to be explored is in Anderson localization, which is the focus of this project.

The Anderson model is set on a lattice, which in Anderson's original paper (Anderson [1958]) is three-dimensional, with a given site denoted by j. The evolution of the wave function ψ is described according to this particular Schroedinger equation

$$i\dot{\psi}_j = E_j\psi_j + \sum_{k\neq j} V_{jk}\psi_k, \tag{2.22}$$

with the reduced Planck constant set to unity, $\hbar = 1$. A particle at site j on the lattice has energy E_j which is a stochastic variable uniformly distributed in $[-w, w]$, and the matrix element that describes the interaction between sites is given by V_{jk} which is responsible for the transfer of particles between each site. Note that V_{jk} could also be a stochastic variable with a probability distribution (Anderson [1958]).

The idea is to place a single particle at some initial position at time $t = 0$, and then the propagation of the wave function is studied. At large values of disorder w, or when the density of states is low, no diffusion can occur leading to Anderson localization where the probability distribution remains localized in a small region of space. Anderson also found an estimate of the critical density, the density at which Anderson localization does not occur, and any density higher than this leads to the diffusion of the wave function (Anderson [1958]). We note that in one dimension there is no transition and therefore no critical state. Indeed, Abrahams et al. [1979] presented a scaling theory of localization, with the scaling function for a sample of size L^d given by the logarithmic derivative

$$\beta(g) = \frac{d\ln(g)}{d\ln(L)}, \tag{2.23}$$

where g is the dimensionless conductance and d is the spatial dimension. This

hypothesis leads to the following conclusions; that there exists a metal-insulator transition originating from the disorder in the system in three dimensions, and that in two dimensions or less no metal-insulator transition occurs (Brandes and Kettemann [2003]).

The region that the majority of the wave function is localized within is known as the localization length. Suppose the wave function at the Fermi level behaves like

$$|\psi(x)| \propto \exp(\frac{-|x - x_0|}{\xi}), \tag{2.24}$$

with ξ the localization length. So at $0K$ the current is carried by the electrons at the Fermi level, and if an electron wave packet is put into the system it can diffuse only over a distance ξ. Hence, the system behaves like a conductor if the system size is much less than the localization length, and it behaves like an insulator if the system size is much larger than the localization length (Brandes and Kettemann [2003]). The Thouless formula gives an estimate of the localization length for systems with weak disorder and within the energy band $-E_B < E < E_B$ defined by the zero disorder, with $E_B > 0$ representing the energy at the band edge. The Thouless formula is given by

$$\xi \approxeq \frac{24(4 - E^2)}{w^2} \tag{2.25}$$

when off the band centre, and

$$\xi(E = 0) \approxeq \frac{105}{w^2} \tag{2.26}$$

when at the band centre (M. Izrailev et al. [2011]).

2.3 Lyapunov Exponents

From the output of the simulation, the trajectories (x, t) given in the form of a time series can be studied. Certain properties of the system could be identified that go beyond what the wave function shows in the normal quantum theory for the Anderson model, so finding a way to characterise their behaviour seems like an appropriate place to start. Looking for chaotic behaviour in the trajectories should help to accomplish this. In order to characterise whether a given trajectory is chaotic, techniques in non-linear dynamics need to be considered. One such way to determine chaos is to estimate the maximal Lyapunov exponent (MLE) of a trajectory.

Lyapunov exponents give a measure of the mean rate of divergence of perturbed trajectories which start infinitesimally close to an unperturbed trajectory.

The idea is to study a single trajectory $x(t)$ by looking at how the perturbed trajectories $x_\epsilon(t)$ evolve, with $x(0)$ and $x_\epsilon(0) = x(0) + \delta x(0)$, $\epsilon = |\delta x(0)| \ll 1$ the initial conditions. If the distance $\Delta(t)$ between the perturbed and unperturbed trajectories either remains bounded or grows algebraically then the system is a non-chaotic one. If it grows exponentially with time as per

$$\Delta(t) \sim \epsilon \exp(\lambda t), \tag{2.27}$$

then the system is chaotic. Here λ is the local exponential rate of expansion. Keep in mind that this is true only asymptotically, so a more precise definition is required for the expansion rate. Most commonly, the MLE is found since this provides an indication of the predictability for a given dynamical system. A positive, finite MLE implies a chaotic system. An equation for the MLE is given below in the form of a double limit (Vulpiani [2010]).

$$\lambda_{max} = \lim_{t\to\infty} \lim_{\epsilon\to 0} \frac{1}{t} \ln\left(\frac{|x(t) - x_\epsilon(t)|}{\epsilon}\right). \tag{2.28}$$

We note that exponential divergence sets in only after some transient time, since an arbitrary difference vector has to turn into the most unstable direction. With this in mind, define the maximal effective exponent λ_τ, in analogy to equation (2.28), as

$$\begin{aligned} \lambda_\tau(t) = \lim_{\epsilon\to 0} \frac{1}{\tau} \ln\left(\frac{|x(t+\tau) - x_\epsilon(t+\tau)|}{\epsilon}\right), \\ x(t) - x_\epsilon(t) = \epsilon w_u(t). \end{aligned} \tag{2.29}$$

Here $w_u(t)$ represents the local eigenvector associated with λ_{max}. By definition the average of $\lambda_\tau(t)$ along the trajectory is the true MLE.

Suppose we have m-dimensional delay coordinates: $\mathbf{x}_t = (x_{t-m+1}, ..., x_t)$, with t an arbitrary time index. Define the embedding dimension m as the dimension of the delay coordinate space. Delay coordinates are simply the one dimensional time series arranged into an m-dimensional space, with each axis representing the time series with a different starting point in time. So we define delay vectors as vectors in delay coordinates. All delay vectors of the time series falling into the ϵ-neighbourhood U_t of $\mathbf{x}_t$ will be considered as the beginning of neighbouring trajectories, the rest of which is formed by consecutive in time entries of the time series. After a transient time, when the difference vector points in the most unstable direction, when measuring their distance in true phase space the rate of divergence

fluctuates exactly as described by the distribution of effective Lyapunov exponents.

Define the distance between a reference trajectory $\mathbf{x}_t$ and a neighbour $\mathbf{x}_i$ after the relative time τ as

$$dist(\mathbf{x}_t, \mathbf{x}_i; \tau) = |x_{t+\tau} - x_{i+\tau}|, \tag{2.30}$$

so as not to distinguish any particular embedding dimension m (Kantz [1994]).

Chapter 3

Methods for the Simulation

The general method for the simulation, set on a one-dimensional grid, goes as follows. First the wave function and trajectory initial positions are set, along with initializing the evolution methods and the constant in time potential energy. Then at each time step the wave is propagated and the absorbing potential is applied, if applicable, followed by the evolution of the trajectories. After that, some variables are calculated such as the quantum potential and quantum entropy. The output is then written, which stores the positions of the particles, along with the amplitude and phase of the wave at each x point for that time step.

The program has many different propagation methods for both the wave and trajectories which can account for many different situations, but for the Anderson model updating the wave via the Chebyshev propagation method is ideal due to its reputation for being accurate. Using the Chebyshev propagation method requires that the dispersion relation be of type $\cos(k)$, meaning that updating the trajectories via local integration is required due to the other methods assuming a k^2 dispersion relation.

3.1 Wave Propagation

The details of the wave propagation methods used in the program, Fourier propagation and Chebyshev propagation, are explained here along with a small discussion on their differences compared to the other method.

3.1.1 Fourier Propagation

The Fourier propagation method involves transforming into Fourier space and propagating the wave function from there before applying the inverse Fourier trans-

form. The aim is to apply the time evolution operator to the wave function, so $\psi_{n+1} = U(dt)\psi_n$ where ψ_n is ψ at time point n and $U(dt)$ is the time evolution operator,

$$U(dt) = \exp\left(\frac{-idtH}{\hbar}\right), \tag{3.1}$$

with dt the spacing between time points, H the Hamiltonian, and $\hbar$ the reduced Planck constant. Keep in mind that $\hbar = 1$ in this program. The calculation for wave function propagation is split into two parts,

$$\psi' = \exp\left(\frac{idt}{2m}\frac{\partial^2}{\partial x^2}\right)\psi_n, \tag{3.2}$$

$$\psi_{n+1} = \exp(-idtV)\psi', \tag{3.3}$$

which gives the time evolution operator from equation (3.1) using $H = \frac{-1}{2m}\frac{\partial^2}{\partial x^2} + V$ as the Hamiltonian, with V representing the potential and m the mass of the particle.

The part represented by equation (3.2) is calculated by transforming $\psi(x,t)$, the wave function at position x and time t, into Fourier space. This is done using a Fast Fourier Transform (FFT) algorithm on the wave function, giving $\tilde{\psi}(k,t)$ which is the wave function in Fourier space at position k and time t. From here part of the time evolution operator is applied, where the advantage of applying the Fourier transform becomes clear. The second derivative operator can be replaced by a coefficient which depends on the position k in Fourier space under consideration. This can be shown by taking the second derivative of an inverse Fourier transform,

$$f(x) = \int_{-\infty}^{\infty} \tilde{f}(k)e^{ikx}dk, \tag{3.4}$$

$$\frac{\partial^2}{\partial x^2}f(x) = \int_{-\infty}^{\infty} -k^2\tilde{f}(k)e^{ikx}dk, \tag{3.5}$$

with $f(x)$ being an arbitrary function.

Therefore differentiating with respect to x twice in x-space is equivalent to multiplying each $\tilde{f}(k)$ term by $-k^2$. Hence when applying this part of the time evolution operator to each $\tilde{\psi}(k,t)$ replace $\frac{\partial^2}{\partial x^2}$ with the coefficient $a(k) = -k^2$. After evolving $\tilde{\psi}(k,t)$ in Fourier space, we take the inverse Fourier transform also with a FFT algorithm to get $\psi'(x,t)$.

Part two, represented by equation (3.3), is easily calculated in x-space by finding the value of the potential V at each x point and substituting into the ex-

ponential for the corresponding $\psi'(x,t)$. This calculation gives the fully propagated wave at the next time step, which is $\psi(x,t+dt)$.

3.1.2 Chebyshev Propagation

This wave propagation method requires a different dispersion relation to the one usually used for Fourier propagation. The usual dispersion relation given by

$$E = \frac{k^2}{2m} \tag{3.6}$$

will be referred to as the k^2 dispersion and the dispersion relation needed for Chebyshev propagation to work given by

$$E = \frac{1-\cos(k)}{m} \tag{3.7}$$

will be referred to as the $\cos(k)$ dispersion. Note that it is also possible to use the Fourier propagation method for $\cos(k)$ dispersion, after a change in the time evolution operator. Here, E is the kinetic energy of the wave-particle system, k is the wave number and m is the rest mass. The reduced Planck constant $\hbar$ was set to unity.

First, the time evolution operator $U(\tau) = \exp(-iH\tau)$ is expanded into Chebyshev polynomials of first kind. The Hamiltonian is required to be rescaled to the interval $[-1,1]$ applicable for Chebyshev polynomials T_k, which gives $H = a\tilde{H}+b$. The time evolution operator can then be rewritten as

$$U(\tau) = \exp(-ib\tau)\left[c_0(a\tau) + 2\sum_{k=1}^{M} c_k(a\tau)T_k(\tilde{H})\right], \tag{3.8}$$

where $c_k(a\tau) = (-i)^k J_k(a\tau)$ are the Chebyshev coefficients, with J_k representing the first-kind Bessel function of order k. To evolve the wave function from one time point to the next, we perform $|\psi(\tau+\Delta\tau)\rangle = U(\Delta\tau)\,|\psi(\tau)\rangle$ which requires finding $|v_k\rangle = T_k(\tilde{H})\,|\psi(\tau)\rangle$ for each k. Rather than using this relation to calculate each $|v_k\rangle$, they are calculated by taking advantage of the Chebyshev polynomial recurrence relation, given by

$$|v_{k+1}\rangle = 2\tilde{H}\,|v_k\rangle - |v_{k-1}\rangle\,, \tag{3.9}$$

with $|v_1\rangle = \tilde{H}\,|v_0\rangle$ and $|v_0\rangle = |\psi(\tau)\rangle$. One feature of the Bessel functions is their fast asymptotic decay,

$$J_k(a\tau) \sim \frac{1}{\sqrt{2\pi k}} \left(\frac{ea\tau}{2k}\right)^k, k \longrightarrow \infty, \tag{3.10}$$

which means that the Chebyshev coefficients vanish quickly. The number of Chebyshev coefficients required is therefore finite, with the number used in the program being 16, so $M = 15$.

For the simulation, the method is initialised by finding the Hamiltonian matrix, and the Chebyshev coefficients can also be found since $c_k(a\Delta\tau)$ depends on the time step and not on time itself. Then in the method itself it is simply a matter of using equations (3.8) and (3.9) (Schubert and Fehske [2008]).

3.1.3 Comparison Between Methods and Setting the Potential

While Fourier propagation is more flexible with which dispersion relation is used, Chebyshev propagation is much more useful due to its ability to get accurate results efficiently. Also, since this method directly involves the Hamiltonian as a matrix it is intuitively easier to set-up the potential for a tight binding model. In this case the potential used would be the Anderson potential which replicates the Anderson model, with the Hamiltonian matrix set as in equation (2.22). So the input disorder w sets the range of lattice energy values, the diagonal elements of the matrix, with the interaction between sites, which is only between neighbouring sites, being identical at every site. Therefore the Chebyshev propagation method is used to obtain results relating to the Anderson model, though Fourier propagation is still useful in this project for testing the simulation for zero potential.

3.2 Boundaries

The code has three boundary types which are absorbing, hard-wall and periodic boundaries. To clarify, the absorbing boundaries are where the wave is absorbed nearly completely in an attempt to mimic the grid of x-positions being part of an infinite region. Hard-wall boundaries involve the wave being completely reflected back and periodic boundaries allow the wave (and all trajectories) to emerge at the other side of the grid.

The theory behind the implemented absorbing boundaries is described in an article by Kosloff and Kosloff [1986]. The basic idea is to have the reduction factor at its largest at the boundary and to then taper it off as the grid points under consideration get further from the boundary. This tapering is done to avoid unwanted reflections. So, an amplitude reduction step after the wave has propagated

is included, which is a forward differencing step described by

$$\psi = (1 - \gamma dt)\psi^{(0)}. \tag{3.11}$$

The reduction function γ is given by

$$\gamma = \frac{U_0}{\cosh^2(\alpha.n)}, \tag{3.12}$$

with U_0 a constant, α a decay factor and n the number of grid points from the boundary.

Note that equation (3.11) can be obtained from

$$\frac{\partial \psi}{\partial t} = -\gamma\psi \tag{3.13}$$

by using a first order time propagation scheme. By comparing equation (3.13) to the time dependant Schroedinger equation it becomes clear that the amplitude reduction step is equivalent to applying a complex absorbing potential. By varying U_0 and α the absorbing potential can be optimised such that transmissions, where parts of the wave travel periodically through the boundary, and reflections are minimised. A balance needs to be found between the number of relevant grid points in the absorbing region which significantly reduce the wave amplitude and sufficient reduction of the amplitude for the wave numbers within this wave. Determining the values of U_0 and α such that reflections and transmissions of the wave at the boundary were minimal ended up being a process of trial and error. Eventually the values were settled on $U_0 = 1$ and $\alpha = 0.18$, which eliminates almost all of the wave amplitude.

For Fourier propagation, which is the method where the wave function is transformed to Fourier space and then propagated, the boundaries are naturally periodic with no absorbing potential. For Chebyshev propagation the boundaries are naturally hard-wall, so periodic boundaries were implemented for this method.

When using the Chebyshev propagation method, and applying the Chebyshev polynomial recurrence relation (3.9), the only calculation to be wary of when considering periodic boundaries is when the rescaled Hamiltonian is applied to a vector. The length of each vector $|v_k\rangle$ in the simulation is equal to the number of grid points in position space N, since we have $|v_0\rangle = |\psi(x,\tau)\rangle$ with $\psi(x,\tau)$ being a vector with length N. Hence, using the Chebyshev polynomial recurrence relation (3.9), all $|v_k\rangle$ are vectors of length N. So when creating a periodic boundary, the lattice points now have to consider lattice hopping for grid points beyond the boundary. Since the rescaled Hamiltonian matrix is tridiagonal, in other words we only

need to consider hopping between nearest neighbours, we just need to involve one lattice point beyond the periodic boundary. Thus an extra two entries to the vectors $|v_k\rangle$, and an extra two rows and columns for the rescaled Hamiltonian matrix $\tilde{H}$, are required for calculating $\tilde{H}\,|v_k\rangle$. An example of how this is done is shown for a system with three grid points, which involves a 3x3 rescaled Hamiltonian matrix $\tilde{H}$ and a 3x1 vector $|v_k\rangle$. The term $tHop$ describes the interaction between sites, which is the same for all lattice points in the simulation.

$$\tilde{H} = \begin{bmatrix} H_{1,1} & tHop & 0 \\ tHop & H_{2,2} & tHop \\ 0 & tHop & H_{3,3} \end{bmatrix} \longrightarrow \begin{bmatrix} H_{3,3} & tHop & 0 & 0 & 0 \\ tHop & H_{1,1} & tHop & 0 & 0 \\ 0 & tHop & H_{2,2} & tHop & 0 \\ 0 & 0 & tHop & H_{3,3} & tHop \\ 0 & 0 & 0 & tHop & H_{1,1} \end{bmatrix}, \tag{3.14a}$$

$$|v_k\rangle = \begin{bmatrix} v_1 \\ v_2 \\ v_3 \end{bmatrix} \longrightarrow \begin{bmatrix} v_0(=v_3) \\ v_1 \\ v_2 \\ v_3 \\ v_4(=v_1) \end{bmatrix}. \tag{3.14b}$$

To apply the Chebyshev propagation method for periodic boundaries we initially extend the vectors and the rescaled Hamiltonian matrix as in (3.14a) and (3.14b), then the method is done as normal except when calculating $\tilde{H}\,|v_k\rangle$. After applying ordinary matrix multiplication the end values are also updated before any further calculations are done. So in the example, for (3.14b), we set $v_4 = v_1$ and $v_0 = v_3$. In this way the effect of periodic boundaries is created.

Lastly, an attempt at making Fourier propagation hard-wall was made by trying to replicate an infinite potential well, adding large values of potential at each end of the grid. This however affects the phase too much, which is not ideal for trajectories whose motion depends on it.

3.3 Evolution of Trajectories

The evolution of the trajectories is forced to be done via local integration due to the $\cos(k)$ dispersion relation previously mentioned, with the other methods taking advantage of the k^2 dispersion relation. This is a simple method which only uses

first order information.

Note that ∇S cannot be found directly from the wave function via

$$\nabla S = \frac{(S_{i+1} - S_{i-1})}{2dx}. \tag{3.15}$$

This is due to the periodic nature of the phase $S(t)$, so if equation (3.15) is used then the value of $(S_{i+1} - S_{i-1})$ could be wrong by $2\pi n$ for some integer n.

Instead we do the following. For each trajectory, the x position is used to find the closest x grid point. Then $\nabla\psi$ and $\nabla\psi^*$ are found using

$$\nabla\psi^{(*)} = \frac{(\psi^{(*)}_{i+1} - \psi^{(*)}_{i-1})}{2dx} \tag{3.16}$$

along with $|\psi|^2$, after which ∇S can be calculated with

$$\nabla S = \frac{Im[\psi^*\nabla\psi - \psi\nabla\psi^*]}{2|\psi|^2}. \tag{3.17}$$

Now $\Delta x = \frac{\nabla S}{m}dt$ is used to update the x position. Equation (3.17) can be found by substituting $\psi = R\exp(\frac{iS}{\hbar})$ into the right hand side, noting that $\hbar = 1$ in this program. So we calculate $\psi^*\nabla\psi$ and $\psi\nabla\psi^*$ which gives

$$\psi^*\nabla\psi = R\exp(-iS)[(\nabla R)\exp(iS) + Ri\nabla S\exp(iS)] = R\nabla R + iR^2\nabla S, \tag{3.18a}$$

$$\psi\nabla\psi^* = R\exp(iS)[(\nabla R)\exp(-iS) - Ri\nabla S\exp(-iS)] = R\nabla R - iR^2\nabla S. \tag{3.18b}$$

Therefore we get

$$Im[\psi^*\nabla\psi - \psi\nabla\psi^*] = 2R^2\nabla S, \tag{3.19}$$

which can be rearranged to get equation (3.17).

Chapter 4

Methods for Time Series Analysis

4.1 Estimating the Maximal Lyapunov Exponent

This section details a method for estimating the MLE of a particle trajectory, with each trajectory given as a time series output from the simulation. Rather than coding this method from scratch, the TISEAN program (Hegger et al. [1999]) is used which has one subroutine that does this exact computation. The method, and the theory behind it, is given below.

4.1.1 Method of Finding the Maximal Lyapunov Exponent

We use the notation and ideas from section 2.3. To measure the MLE λ_{max}, we first fix t, and then complete the following steps

1. We first search for all neighbours $\mathbf{x}_i$ inside an ϵ-neighbourhood U_t of $\mathbf{x}_t$.
2. We then compute the average of the distances between all neighbouring trajectories and the reference trajectory $\mathbf{x}_t$ as a function of τ. This average contains fluctuations which need to be eliminated by completing the next two steps.
3. We now take the logarithm of these average distances which yields the local effective Lyapunov exponent plus a fluctuation ϕ.
4. We average in t over the full time series, with the local fluctuations ϕ cancelling out and the effective exponents averaged to the true Lyapnuov exponent.

Overall the following calculation is completed, giving

$$S(\tau) = \frac{1}{T}\sum_{t=1}^{T} \ln\left(\frac{1}{|U_t|}\sum_{i\in U_t} dist(\mathbf{x}_t, \mathbf{x}_i; \tau)\right). \tag{4.1}$$

Initially the difference vectors in the true phase space are pointing in any direction, so for small τ we cannot expect a scaling behaviour, with the distance behaving like $dist = \sum_i a_i e^{\lambda_i t}$, where λ_i are the effective Lyapunov exponents in the different stable and unstable directions.

In the intermediate range of τ, called the scaling region, $S(\tau)$ increases linearly with its slope equal to the MLE. In this range, τ is large enough for nearly all distance vectors to point in the unstable direction, while the distances are smaller than the size of the attractor. An attractor is a set of numerical values toward which a system tends to evolve, for a wide variety of starting conditions of the system. System values close enough to the attractor values remain close even if slightly disturbed (Strogatz [2007]).

For large τ, distances are close to the size of the attractor and $S(\tau)$ asymptotically tends towards a constant since the distances cannot grow any more.

Therefore, measuring the MLE is as simple as measuring the gradient of $S(\tau)$ in the scaling region. See figure 4.1 for an example. In this example a Henon map is used, a well known chaotic system, with the data created using a subroutine from the TISEAN program. Some noise is artificially added to the data using a function also included in TISEAN, to observe how TISEAN could cope with noise from a real time series when measuring the MLE. The measured MLE gives a good approximation to the known analytical solution of ln(2) as demonstrated by Sprott [2007].

4.1.2 Embedding Dimension, Neighbourhood Size and Noise

If the time series data is noisy then the typical distance between two neighbouring trajectories is of the order of the noise level. If ϵ is chosen which is smaller than the noise amplitude, and neighbours are found for this value, then $S(\tau)$ jumps from a value smaller than $\ln(\epsilon)$ to a value given by the noise level at $\tau = 1$. If this value is not too large, one can still find a scaling range and the exponent thus found is not too affected by the noise. Hence, it is required that there is a balance between a smaller ϵ to reduce the effects of noise and a larger ϵ so that he number of nearest neighbours is large enough. This is why various different sizes of ϵ are sampled in TISEAN.

Trying different values of embedding dimension m, the dimension of the delay coordinate space (see section 2.3), is also useful because of the following reason. If m is too small then there is a non-zero probability that two trajectories are close in the embedding space but not in the true phase space. In this case their distance increases strongly until τ is large enough such that $\tau + m$ is a good embedding. From this point on increase in distance is again determined by λ_{max}. However, the

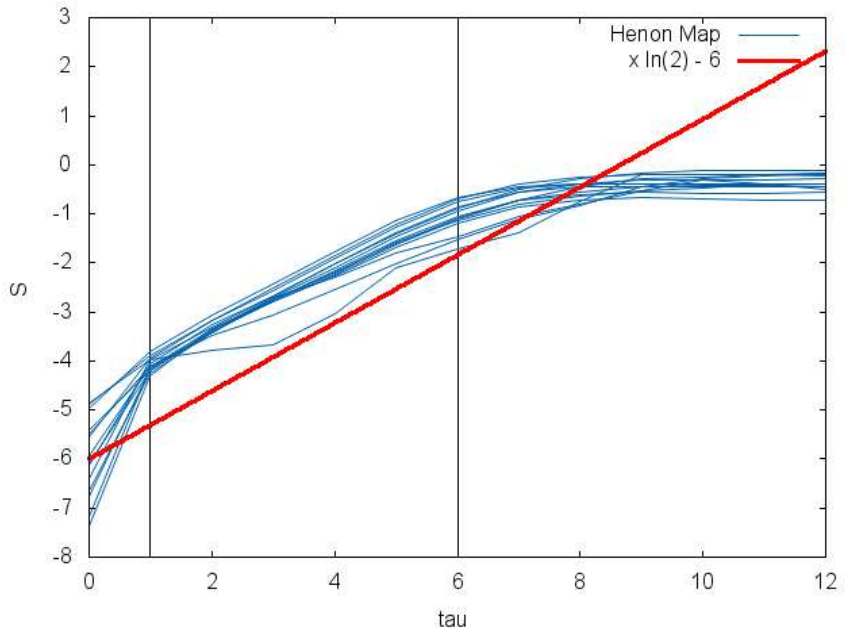

Figure 4.1: An example of a typical $S(\tau)$ plot. For τ in the range 1–6, the linear part of the curves are visible. This is the scaling region, and the gradient of these lines give an estimate of the MLE. The red line is used to compare.

distance at this point can already be so large that the scaling region is strongly reduced. To avoid this, different values of m are attempted in TISEAN between an input minimum and maximum (Kantz [1994]).

4.2 Distribution of MLEs

4.2.1 Automating the MLE Estimation

While TISEAN gives a nice method for computing the MLEs, finding the gradient of the scaling region, with the scaling region found by eye, for 101 trajectories would be a lengthy process. That is why a way of finding the scaling region and measuring the gradient for the MLE within a computer program needs to be found for many trajectory plots to be analysed. The way that this is done involves trying trial scaling regions and measuring the variance of a fitted line. Using this variance and the interval of the trial scaling region the fit is given a score, and the region with the best score is determined to be the true scaling region. More detail is given below, with Wolfram Mathematica Version 10.1 used for running this program, analysing the output and producing the plots throughout.

For each trajectory:

1. Read in an input file to get an array S with a given row representing a line of $S(\tau)$, each of which have different neighbourhood sizes or embedding dimensions.

2. Go through each line in the $S(\tau)$ plot.

   (a) Go through the start point of each range to be trialled, which is fixed in length.

      i. Fit a line to $S(\tau)$ within that range.

      ii. Find the gradient of the line and its variance with the points of $S(\tau)$.

      iii. Discard trial scaling regions which have a negative gradient or the variance is too large.

   (b) Score the output list of trial scaling regions (if any are found) according to smallest upper limit of the range of τ, t_{max}, and smallest variance. So the smallest variance gets a score of one, the second smallest a score of two, and so on.

   (c) Then the trial scaling region with the lowest (best) score is used, and if a few are found with equal score then the one with the smallest t_{max} is taken.

3. Check if a trial scaling region is found for any line of $S(\tau)$. If none are found then simply set the range to start at $\tau = 0$.

4. Otherwise find the most common range used by all lines of $S(\tau)$. If there is more than one of these then find their mean average and round to the nearest integer. This is the final range used for all lines of $S(\tau)$.

5. Find the gradient of each line of fit for this final range, and also their variance.

6. Find the mean average of these gradients to be used as the final estimate of the MLE.

7. Find the standard error of the regression slope using the mean average of the variance as the variance used in the equation: $S_{err} = \sqrt{variance}/\sqrt{\sum_i (x_i - \bar{x})^2}$. This can be used for error bars to see if the estimated MLE is from a good fit. See Appendix A for more details.

8. Output the MLE and the standard error of the regression slope, along with the range used for the scaling region, for each trajectory.

The output can be checked using an $S(\tau)$ plot with the fitted line, also showing the scaling region used, for each trajectory as in figure 4.1. A plot of MLE against trajectory initial position can be shown, also with error bars from the standard error of the regression slope, and the data is printed for further analysis.

4.2.2 MLE Histograms

Since it is now possible to study a lot of trajectories quickly in terms of their MLE, using the aforementioned program, each trajectory can be analysed again in different realisations for the same value of disorder. In the simulation this is done by changing the seed for the random number generator, so that the Anderson potential has different random values for the lattice site energies. So for 100 realisations of the system, the MLE of 101 trajectories can be found. Then distributions of the MLE for each trajectory can be plotted, and a plot of average MLE against the trajectory initial position can be shown for a given value of disorder.

4.3 Distributions from the Trajectories

The set of trajectories from each run of the simulation can be analysed in the form of histograms, which can show the distribution of either trajectory final position or their average velocity over the simulation time. Wolfram Mathematica Version 10.1 is used for plotting.

The final position of each trajectory is recorded and used in the data for a histogram of final positions. This is done for each value of disorder, which leads to a stack of histograms which can be shown in one three-dimensional plot. The mean average of the final position is also found for each value of disorder, which can also be shown on the final plot. This can be used to test that the Born rule holds by initialising the trajectories according to the Born rule probability distribution. The distribution of trajectories can be compared at the end of the simulation, using these final position histograms, to the probability distribution given by the Born rule.

For each trajectory the average velocity over the total time is found, and this is also done for the average velocity over the final 2000 time steps to give an idea of the final velocities of each trajectory in general. These can be used to produce histograms of average velocity. The mean of these average velocities per value of disorder can also be calculated and shown alongside the three-dimensional stack of the two-dimensional histograms in the final plot shown.

Chapter 5

Results and Discussion

This chapter presents and discusses the results from the output of the simulation, for the three main sections of the program which are wave propagation, boundaries and Bohm particle evolution. Also shown and analysed are the results relating to the MLEs of trajectories and histograms showing the distributions of trajectory final positions and average velocities.

5.1 Accuracy of the Simulation

In order to check whether the simulation gives accurate results simple cases are tested, which means zero potential cases which are easy to solve analytically.

5.1.1 Wave Propagation

Figures 5.1, 5.2 and 5.3 all show the output from the simulation for a free wave packet at the centre of the band energy with zero potential, for both the Fourier and Chebyshev propagation methods. The $\langle x \rangle$ calculated analytically is from the k^2 dispersion relation for all plots. The numerically calculated $\langle x \rangle$ is from the relevant dispersion relation, as is the group velocity. The output wave can therefore be compared with the known analytical solution for wave propagation using the k^2 dispersion relation. Use E_0 to represent the centre of the band energy for $cos(k)$ dispersion, as reference. Due to how the simulation is set up, E_0 is not zero as it usually is but is instead a positive value, $E_0 = 2$.

Figure 5.1a shows the analytical $\langle x \rangle$ matching the numerical $\langle x \rangle$, and also the wave amplitude propagates with the velocity predicted by the group velocity found for the k^2 dispersion. This shows that the wave is propagating as expected for the Fourier propagation method and k^2 dispersion relation.

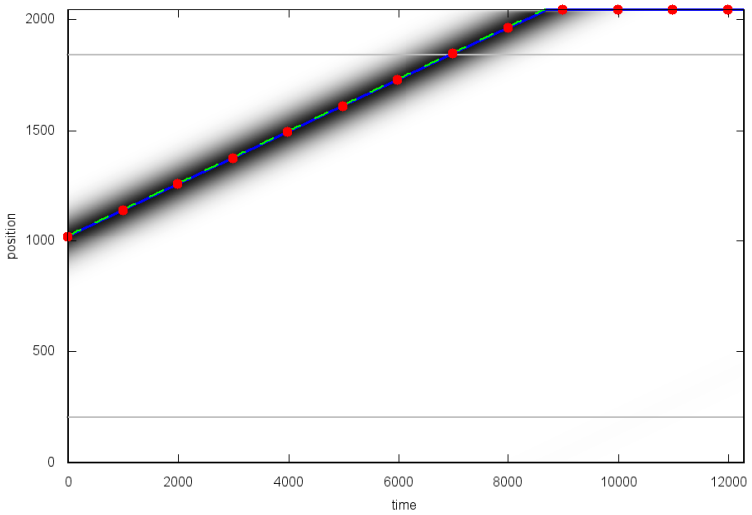

(a) Fourier Propagation - k^2 dispersion - Initial Kinetic Energy = E_0

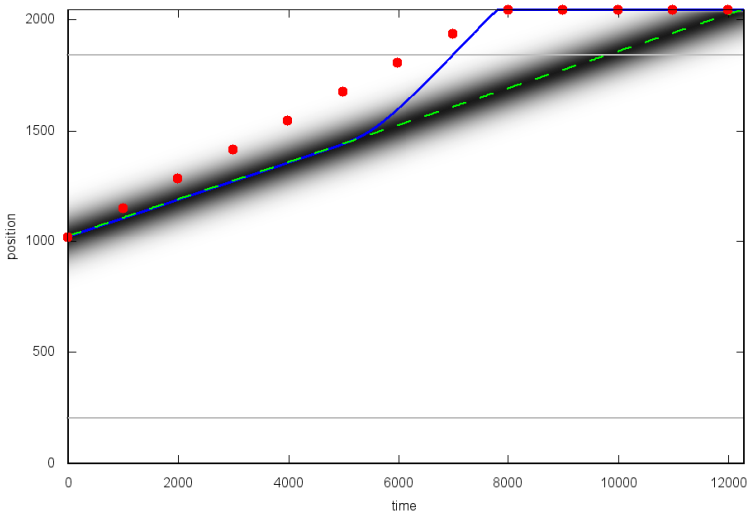

(b) Chebyshev Propagation - $cos(k)$ dispersion - Initial Kinetic Energy = E_0

Figure 5.1: Plots showing the wave function amplitude (dark layer) in one-dimension at each time point, for different dispersion relations. Blue Solid Line = Numerical $\langle x \rangle$. Red Dots = Analytical $\langle x \rangle$. Green Dashed Line = Group Velocity.

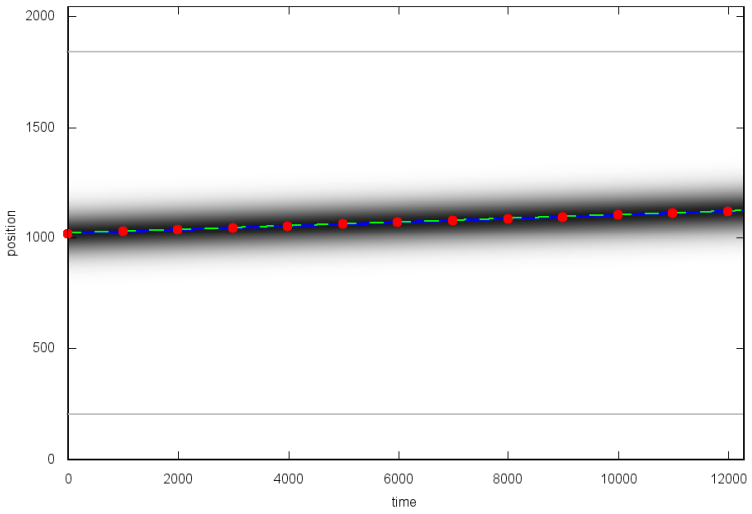

(a) Fourier Propagation - $cos(k)$ dispersion - Initial Kinetic Energy = $0.005E_0$

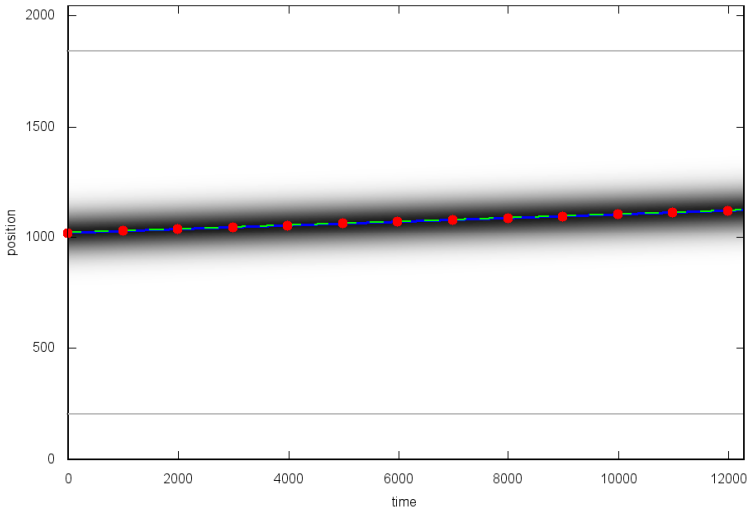

(b) Chebyshev Propagation - $cos(k)$ dispersion - Initial Kinetic Energy = $0.005E_0$

Figure 5.2: Plots showing the wave function amplitude (dark layer) in one-dimension at each time point, for different wave propagation methods. Blue Solid Line = Numerical $\langle x \rangle$. Red Dots = Analytical $\langle x \rangle$. Green Dashed Line = Group Velocity.

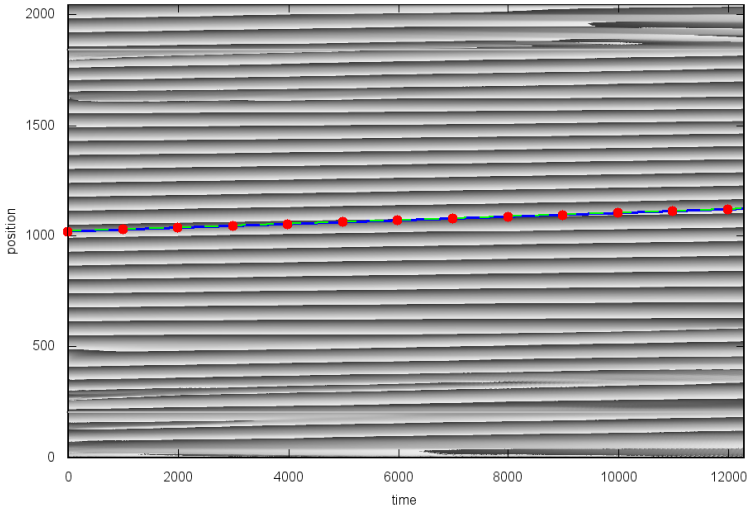

(a) Fourier Propagation - $cos(k)$ dispersion - Initial Kinetic Energy = $0.005E_0$

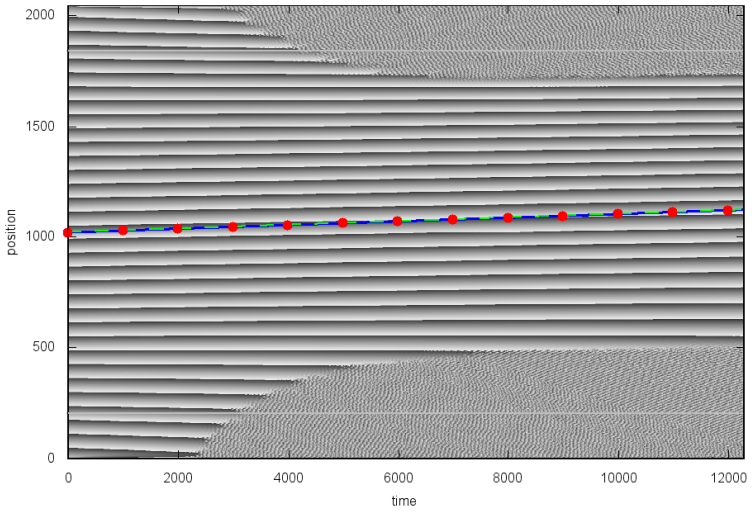

(b) Chebyshev Propagation - $cos(k)$ dispersion - Initial Kinetic Energy = $0.005E_0$

Figure 5.3: Plots showing the phase of the wave function (dark layer) in one-dimension at each time point, for different wave propagation methods. Blue Solid Line = Numerical $\langle x \rangle$. Red Dots = Analytical $\langle x \rangle$. Green Dashed Line = Group Velocity.

Figure 5.1b shows the analytical $\langle x \rangle$ with a completely different gradient to the numerical $\langle x \rangle$ on the plot. This is to be expected, since the initial kinetic energy is relatively large and so the dispersion relations being different becomes apparent. This shows how a wave with the $\cos(k)$ dispersion propagates differently to a wave with the k^2 dispersion. Figure 5.1b suggests that the wave with the $\cos(k)$ dispersion propagates as it should, since the numerical $\langle x \rangle$ is in line with the amplitude of the wave for half of the time, though curiously diverges from this afterwards. This could be due to the propagation method used, since even though absorbing boundaries are used for both, the wave is never fully eliminated. The majority of the left over wave ends up either propagating periodically over the boundary for Fourier propagation, or it is reflected for Chebyshev propagation. This causes differing effects of the wave nearer to the boundary between methods. This effect can be seen in the phase plots in figure 5.3. Also, the group velocity of the wave predicts the velocity of the wave correctly which further suggests that the Chebyshev propagation method is working.

So the wave evolution is fine for the k^2 dispersion, in which only the Fourier propagation method can be used. In order to better determine if the wave is propagating properly for the Chebyshev propagation method it is a good idea to use a smaller initial kinetic energy, since this makes the dispersion relations similar, so that a comparison to the analytical solution of the wave function for the k^2 dispersion is possible. This is what is done for the plots in figure 5.2. Both the propagation methods give near identical amplitude plots, and the analytical $\langle x \rangle$ matches the numerical $\langle x \rangle$ for both plots. In addition, the group velocity for both diagrams predicts correctly the direction of travel of the wave in phase space. Also note the similarity of the phase plots in figure 5.3 for the sections unaffected by the boundaries. All of this proves that the wave propagates correctly for the $\cos(k)$ dispersion, and that a change in propagation method doesn't affect the wave evolution, minus the boundary effects.

5.1.2 Boundaries

The boundaries are demonstrated in the plots of figures 5.4, 5.6 and 5.8 showing how the absorbing, periodic and hard-wall boundaries affect the wave amplitude at each given time step. The phase of the wave function is also shown, due to how important that is for particle evolution, by the plots of figures 5.5, 5.7 and 5.9. All boundaries are shown in a zero potential one-dimensional box, with a grid size of 1024 and the number of time steps set to 12288. The system is evolved for the centre of the band energy ($E = 2$), using the Chebyshev propagation method of the wave function.

Figures 5.6 and 5.7 show that the hard-wall boundaries have the desired ef-

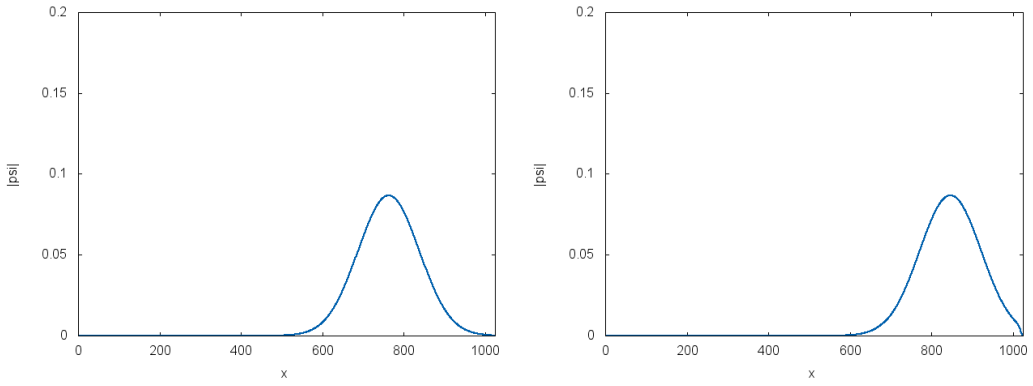

(a) $t = 3000$

(b) $t = 4000$

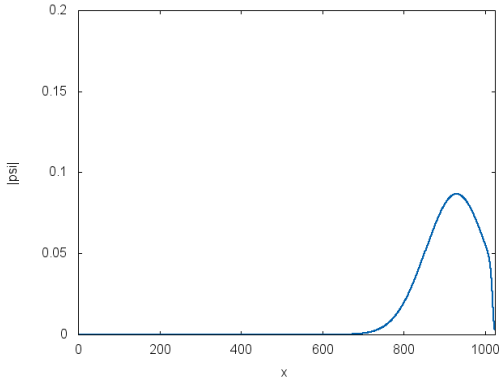

(c) $t = 5000$

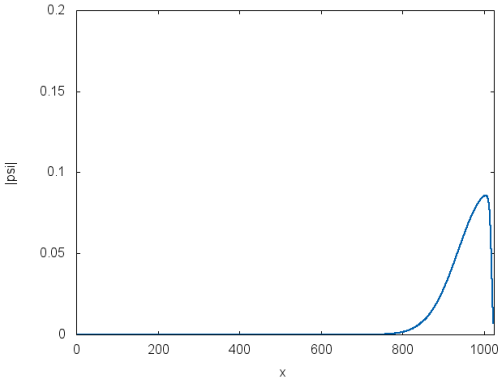

(d) $t = 6000$

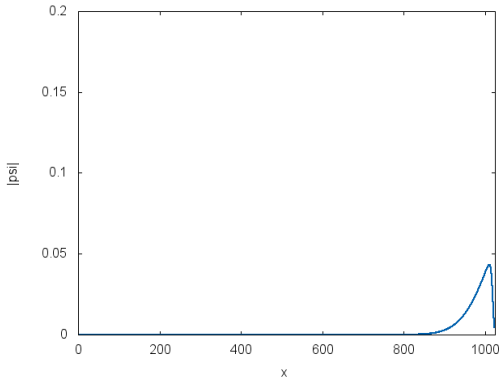

(e) $t = 7000$

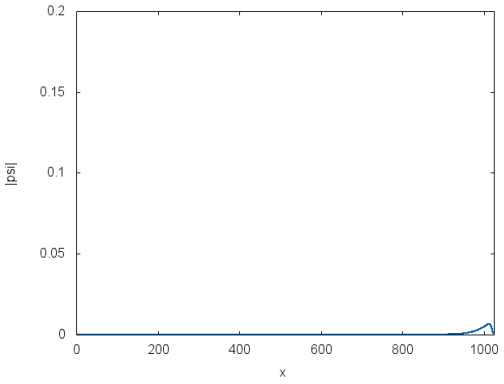

(f) $t = 8000$

Figure 5.4: Plots of wave function amplitude against position at various times, using absorbing boundaries

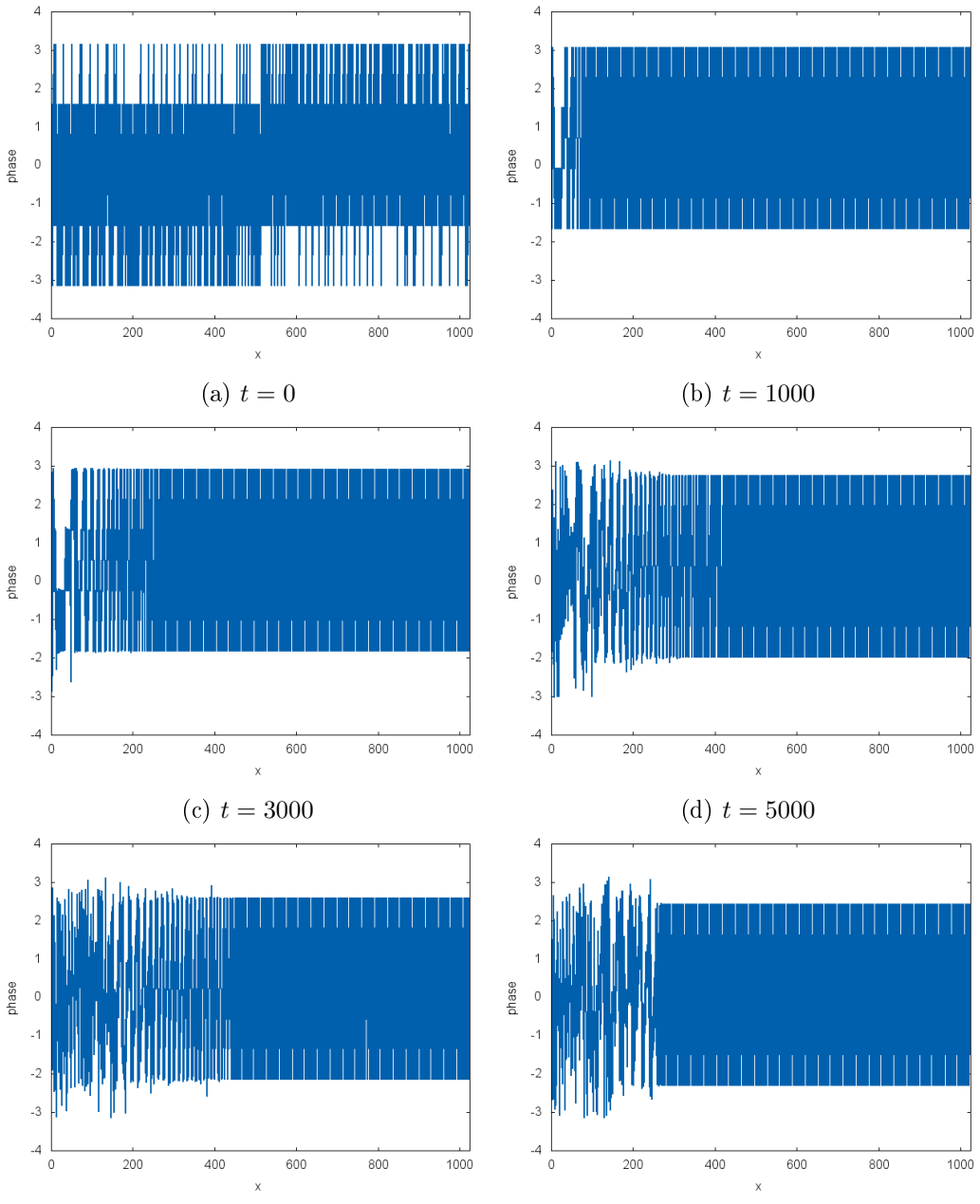

(a) $t = 0$ (b) $t = 1000$

(c) $t = 3000$ (d) $t = 5000$

(e) $t = 7000$ (f) $t = 9000$

Figure 5.5: Plots of the phase of the wave function against position at various times, using absorbing boundaries

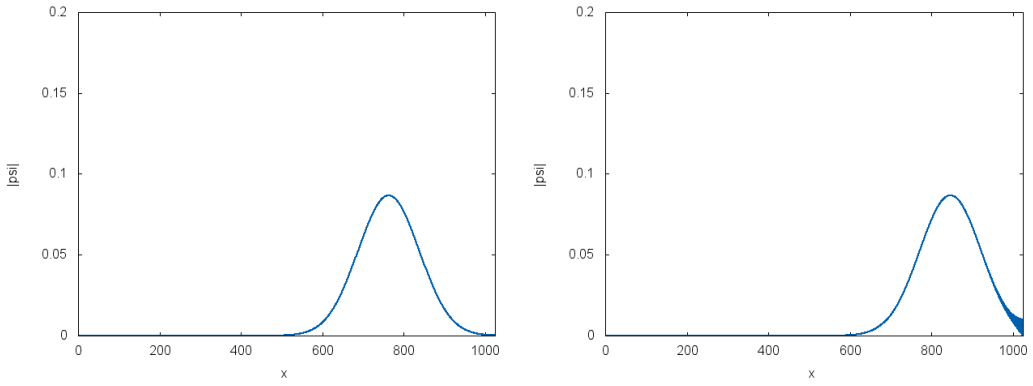

(a) $t = 3000$

(b) $t = 4000$

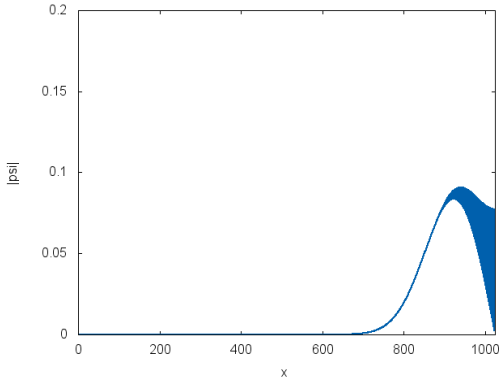

(c) $t = 5000$

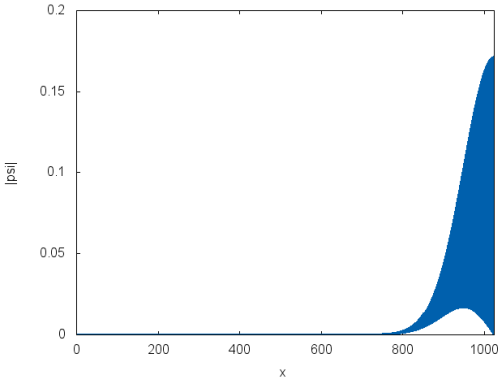

(d) $t = 6000$

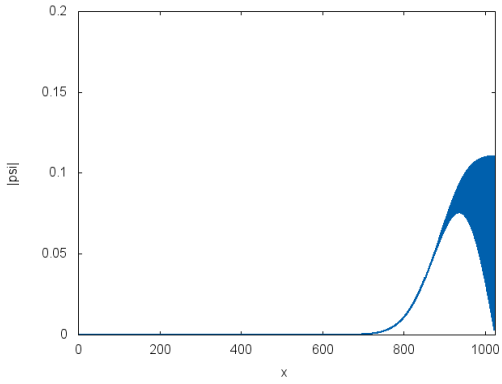

(e) $t = 7000$

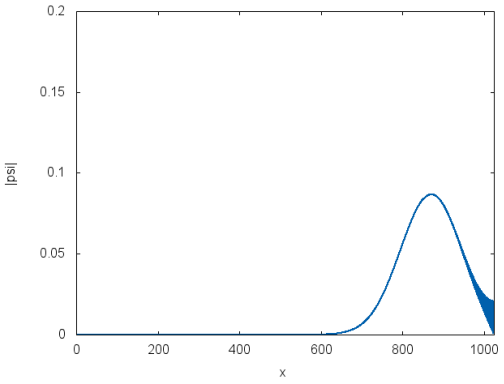

(f) $t = 8000$

Figure 5.6: Plots of wave function amplitude against position at various times, using hard-wall boundaries

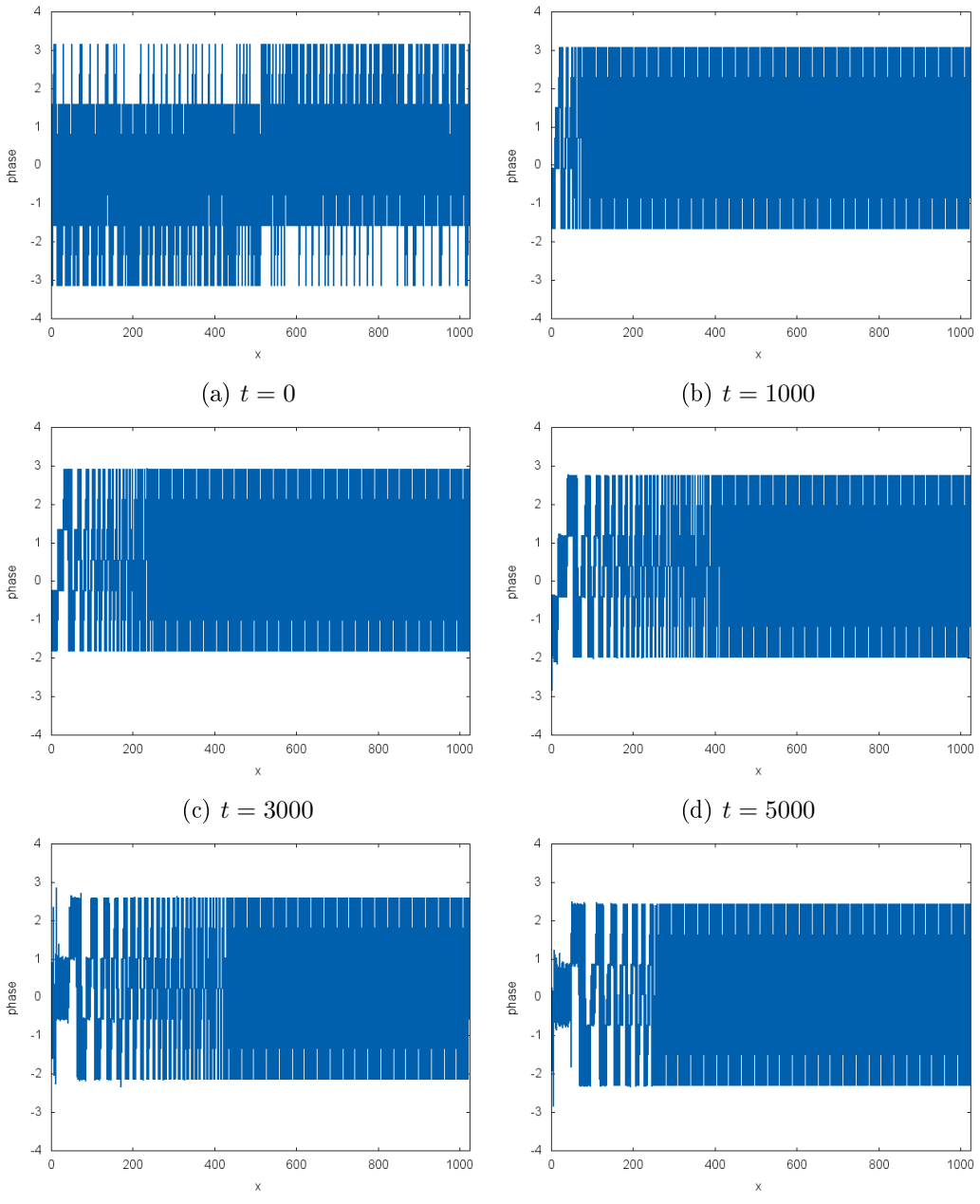

(a) $t = 0$ (b) $t = 1000$

(c) $t = 3000$ (d) $t = 5000$

(e) $t = 7000$ (f) $t = 9000$

Figure 5.7: Plots of the phase of the wave function against position at various times, using hard-wall boundaries

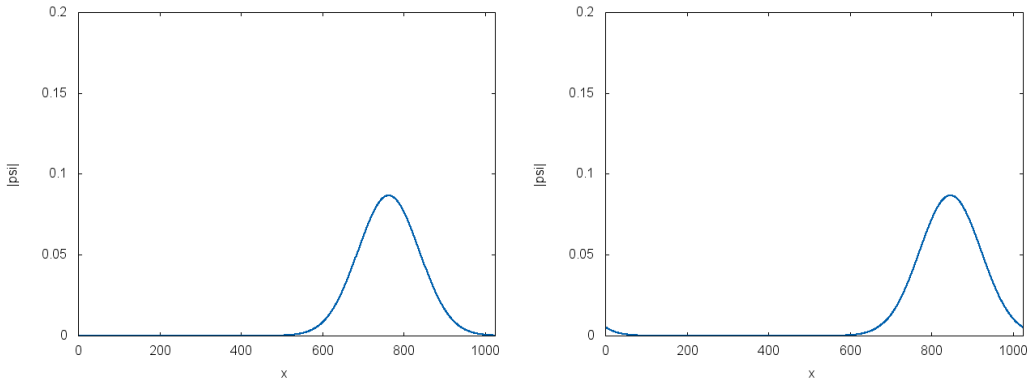

(a) $t = 3000$

(b) $t = 4000$

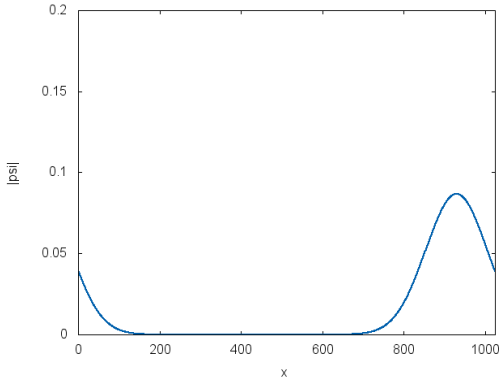

(c) $t = 5000$

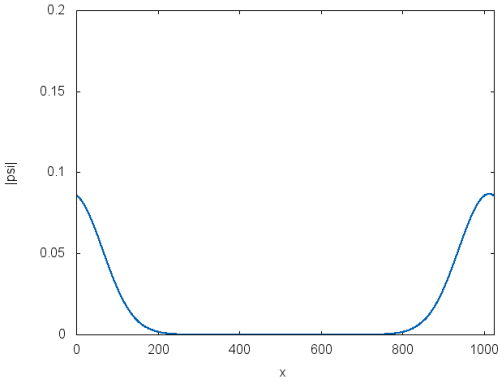

(d) $t = 6000$

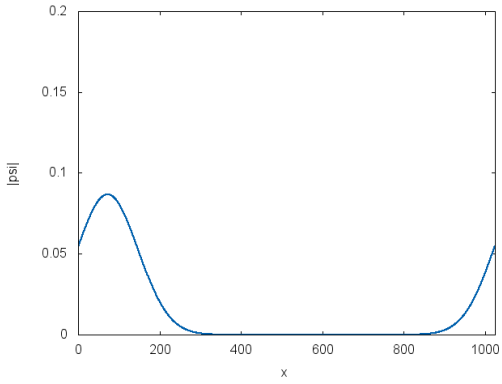

(e) $t = 7000$

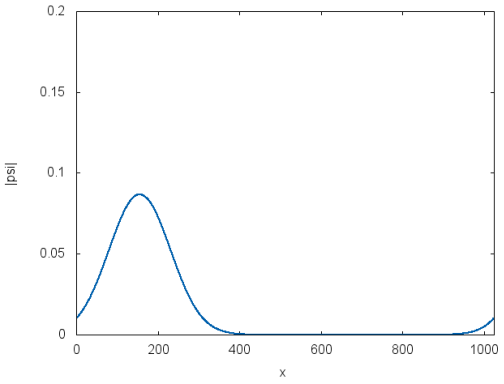

(f) $t = 8000$

Figure 5.8: Plots of wave function amplitude against position at various times, using periodic boundaries

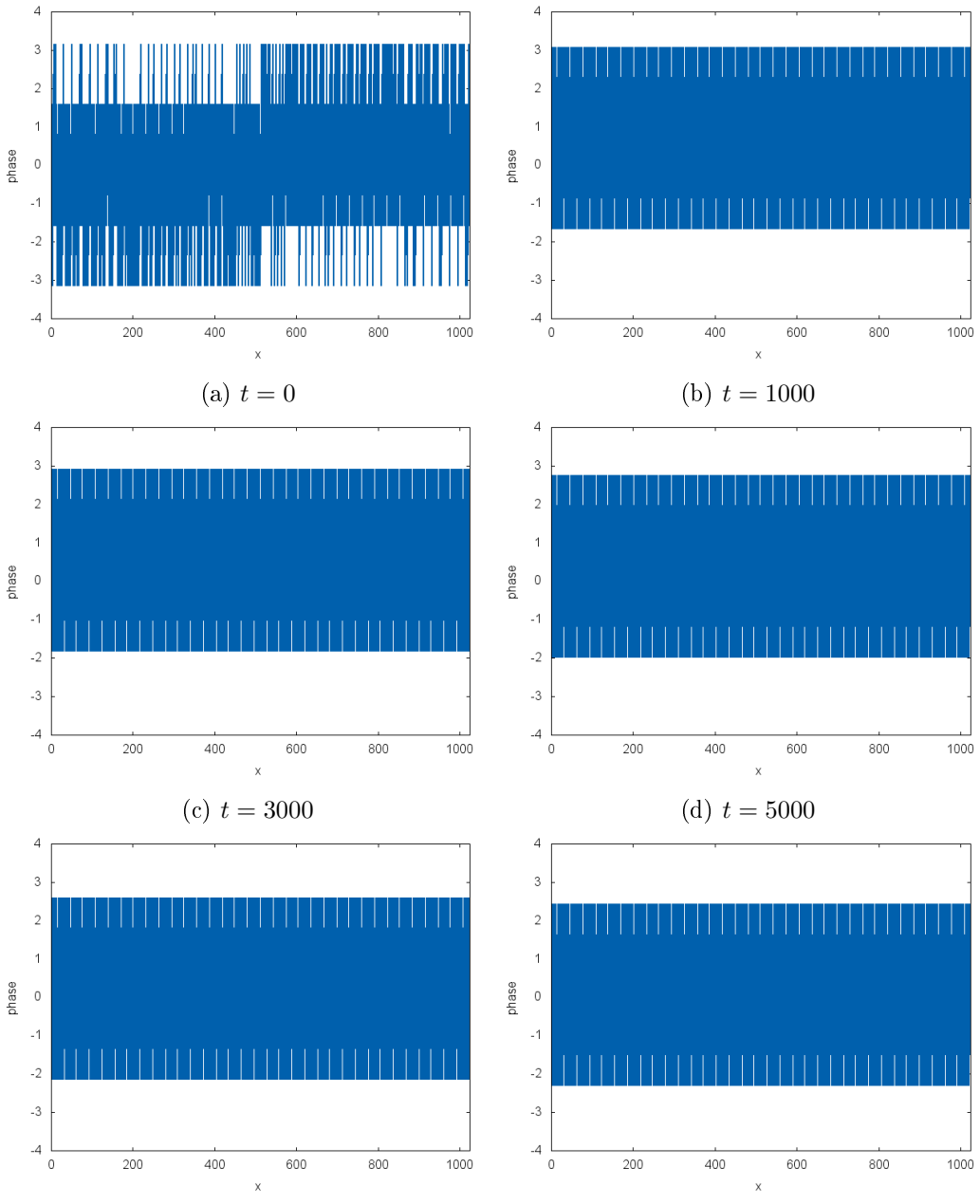

(a) $t = 0$ (b) $t = 1000$

(c) $t = 3000$ (d) $t = 5000$

(e) $t = 7000$ (f) $t = 9000$

Figure 5.9: Plots of the phase of the wave function against position at various times, using periodic boundaries

fect of reflecting the wave, as it should since this is the natural boundary effect for Chebyshev propagation. The phase also shows the wave reflecting, as can be seen with the pattern of the phase reversing direction for $t = 9000$. On a side note, the phase that appears from the boundary in the opposite side of the wave propagation direction appears to be completely different from the initial phase, which is a boundary effect which could alter the paths of trajectories, though most trajectories would be at the other side of the grid in this case. For a non-zero potential and a larger number of time steps this boundary effect, while not necessarily physically incorrect, would have an effect on the paths of the Bohm particles compared to an infinite grid size.

Figures 5.4 and 5.5 show the absorbing boundary effects on a wave packet travelling in zero potential. The idea is to mimic the boundary being just a window, with the wave continuing beyond the boundary, since obviously the simulation grid has to be of finite size. Figure 5.4 appears to show the absorbing boundaries working well for the amplitude, with the boundaries reducing the amplitude of the wave function to zero only for the parts of the wave near to the boundary. The phase appears to act in a similar way to hard-wall, with the phase pattern appearing to reflect off of the boundary. This is showing a tiny portion of the wave not being completely absorbed by the boundary, and since Chebyshev propagation is naturally hard-wall this is why it is only being reflected. This also demonstrates that even though the amplitude is greatly reduced the phase from the tiny portion of the wave function remaining alters the overall phase and could therefore affect the trajectories.

Figures 5.8 and 5.9 shows the periodic boundaries in effect for a Gaussian packet propagating in free space. Both the amplitude and phase of the wave appear to evolve just as intended for periodic boundaries. Additionally the pattern of phase doesn't change much at all, even for the tail end of the wave, since the wave just appears on the other side of the grid rather than the phase appearing somehow from the boundary. This shows that periodic boundaries could be useful for having minimal effect on the phase, with only the wave interfering with itself being a problem, but for a small number of time points this effect would be minimal.

Overall, using periodic boundaries is the best boundary type to go for in terms of affecting the wave function minimally, which can be seen by considering the phase. Hard wall or absorbing boundaries tend to affect the phase in some way, which in turn affects the trajectories. Absorbing boundaries would be perfect if the wave were completely eliminated when absorbed by the boundaries, but if even a small amount of the wave survives then this would affect trajectories due to their reliance on phase and not amplitude. On the other hand, periodic boundaries seem

ideal because they continue the space rather than placing an object at the edge of the simulation grid. They allow the wave to propagate normally, with the only effect appearing due to the wave interfering with itself but this is minimal.

However, absorbing boundaries are used because the plots look more confusing with the trajectories being periodic for periodic boundaries. It would be more difficult to conduct analysis on the localization length using purely the trajectories if the trajectories move from one side of the grid to the other at the boundaries. Absorbing boundaries appear to work well enough anyway, with trajectories near the boundaries not appearing to be too affected. They do not get reflected like they would if the wave reversed direction. Also, before the absorbing boundaries were optimized the trajectories sometimes jumped from one point to another which now does not occur.

5.1.3 Trajectory Evolution

Figure 5.10 shows trajectories for zero potential energy and zero kinetic energy. In this plot the trajectories are initially spaced equidistantly, with the central trajectory being at the centre of the wave and the distance between each trajectory being the rms width of the wave. The wave, which is evolved using Chebyshev propagation, has zero group velocity which implies that the initial velocity of the trajectories must also be zero. Since the dispersion relations are similar for zero kinetic energy, the wave function propagates in the same way for k^2 and $cos(k)$ dispersions. Therefore the analytical solution for the variance found for the k^2 dispersion can be used for the numerical wave using the $cos(k)$ dispersion, and this fact is used in this plot. In order to see the wave spread the simulation runs with a larger number of time points, which means that the grid size must be smaller such that it is possible to plot the results. The rms width of the wave is also made smaller such that it is possible to fit the wave reasonably well within the spatial grid size of 512. This in turn makes the wave spread faster meaning this effect is even more visible on this plot. The number of time steps used is 20000.

Figure 5.10 shows the wave function visibly spreading. The trajectories are expected to stay at the $\sigma(t)$ spacing throughout the simulation, as explained in subsection 2.1.2 in the literature review. Figure 5.10 shows exactly this; the trajectories follow the spreading of the wave predicted analytically. This is a great demonstration that the simulation is working as intended since the wave must be spreading at the correct rate and hence propagating correctly, and also the Bohm particles are being guided properly since they are following the predicted path. There is a small deviation from the expected trajectories which is likely due to the boundary effects;

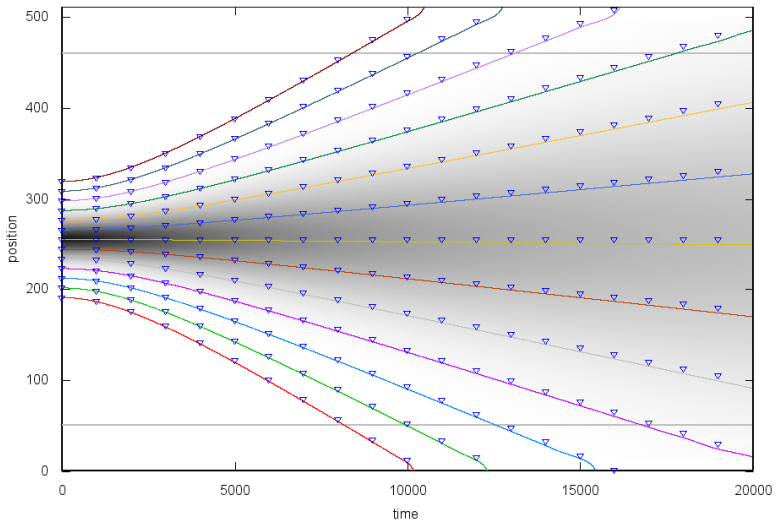

Figure 5.10: This plot shows a visible spreading of the wave function for zero kinetic energy and zero potential energy, with the trajectories initially spaced by the rms width of the wave. The triangular points plotted represent the σ-spacing at every 1000 time steps, found analytically.

in this case the grid size is relatively small so these effects would be more prominent. Also, the wave propagates in the same way for the k^2 and $\cos(k)$ dispersions since the wave has the same dispersion relation for zero kinetic energy. Therefore the previously calculated analytical solution for the rms width of the wave for the k^2 dispersion also works here for the $\cos(k)$ dispersion. This means that an accurate test of the simulation for the $\cos(k)$ dispersion is possible. Given how difficult the analytical solution is to solve without approximations for the $\cos(k)$ dispersion compared to the k^2 dispersion this is a useful test.

5.2 Anderson Localization

Figure 5.11 shows the trajectory plots for the centre of the band energy, while varying the disorder potential for $w = 0.0, ..., 3.0$, with 2048 x points and 12288 time steps used, and with absorbing boundaries. All particles are initially placed equidistantly from each other.

Figure 5.11 gives an intuitive representation of how Bohm particles act for the localized and diffusive states. For $w = 0.0$ the particles and wave evolve in free space, and then for $w = 0.5$ the particles start feeling the effect of the Anderson potential. The top few trajectories carry on as if the potential is still zero, and the central trajectories decelerate quickly and become confined to a small region. Since the trajectories cannot cross the bottom trajectories must decelerate also, and interestingly they get deflected by the disordered potential. These outer trajectories however are initialsed in a region where the amplitude of the wave function is low, so the most likely motions of trajectories according to the Born rule occur in the centre. For $w = 1.0$ the trajectories become even more confined, with even the outer trajectories decelerating. The wave can be seen to be much more confined now and the central trajectories are on average not moving with any velocity. This trend continues from $w = 1.5$ through to $w = 3.0$ where all trajectories are on average motionless and the wave has zero group velocity.

5.2.1 Maximal Lyapunov Exponents

All figures in this section involve 2048 grid points and 12288 time steps in the simulation. When running the program to automate MLE estimation from $S(\tau)$ curves, it is possible to show the plots of $S(\tau)$ with the fitted line and fitting range for each trajectory. This can be used to test if this program works as intended. Some examples of these plots are shown in figure 5.12. The trajectory number refers to the trajectory initial position, with trajectory number 1 referring to the trajectory

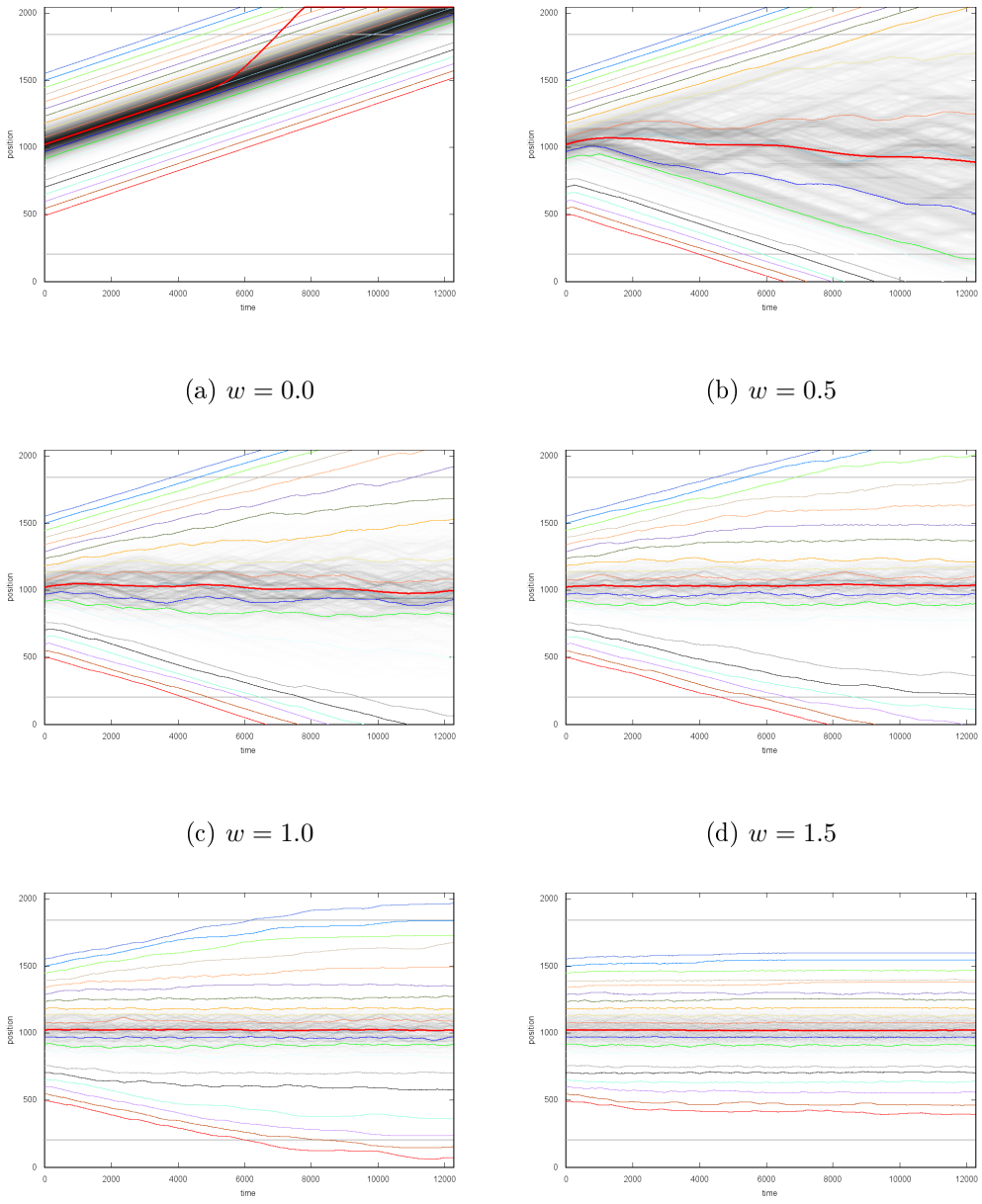

(a) $w = 0.0$ (b) $w = 0.5$

(c) $w = 1.0$ (d) $w = 1.5$

(e) $w = 2.0$ (f) $w = 3.0$

Figure 5.11: Plots showing how the trajectories (multi-coloured lines) change as disorder w is varied. This is done for the centre of the band energy. Thick Red Line = Numerical $\langle x \rangle$.

with the lowest x-position and increasing trajectory number increases the initial x-position. The initial position is given in the sub-captions anyway. All trajectories here were evolved for the centre of the band energy with $w = 0.5$.

Figure 5.12 shows that the scaling regions are much more subtle than one would hope, but the ones found are believable. First, figure 5.12a shows how the program used to find the scaling region can find these regions even if they are small and shallow in gradient, and figure 5.12c shows that it is capable of finding the scaling region when the MLE is zero.

Figure 5.12b shows the program finding the scaling region to be the range of τ values 200–300 approximately, instead of another linear looking part from about 500–1000. This indicates how the program prioritises scaling regions which occur for smaller values of τ, which should be the range selected as the scaling region. In this case it would not be necessarily incorrect to go for the latter range as the scaling region, since finding the scaling region can be somewhat subjective, especially here where the MLEs found are very small.

Figure 5.12d shows an attempt by the program to find the scaling region for a very curved looking $S(\tau)$ plot with no obvious scaling region. The range of τ values 400–1000 seems a good candidate for the scaling region, and the program picks the scaling region to be within this range. The scaling region is chosen to be for the smallest possible τ values, again demonstrating the programs tendency to prioritise this. Figure 5.12e appears to have the scaling region as the τ range 500–1000, and is a very shallow gradient. The program does not have a problem finding the scaling region here, this time choosing a region in the middle of the proposed range. This is probably due to the score given by the variance of the fitted line with the $S(\tau)$ points. So overall the program has the ability to handle most ambiguous cases.

Lastly, figure 5.12f shows the worst case scenario. The $S(\tau)$ plot is unusual, with sudden jumps in values. It could be said that these $S(\tau)$ lines are mostly horizontal and that therefore the MLE is zero. The scaling region chosen by the program however is an unwise choice, landing on one of these discontinuities. The reason that this range is chosen is related to the process of finding the final scaling region. Recall that for each line every possible range is tested as a trial scaling region, and the best one is then picked using the variance of the fitted lines and the size of the values of τ within that range. Once this is done for each line the most common range used by each line is chosen, followed by the mean if there is a tie, for the final scaling region used to find the MLE. The problem comes in when the mean average is used to find the final scaling region, since this allows for the possibility of the mean scaling region falling onto one of these discontinuous points. Since the MLE for this

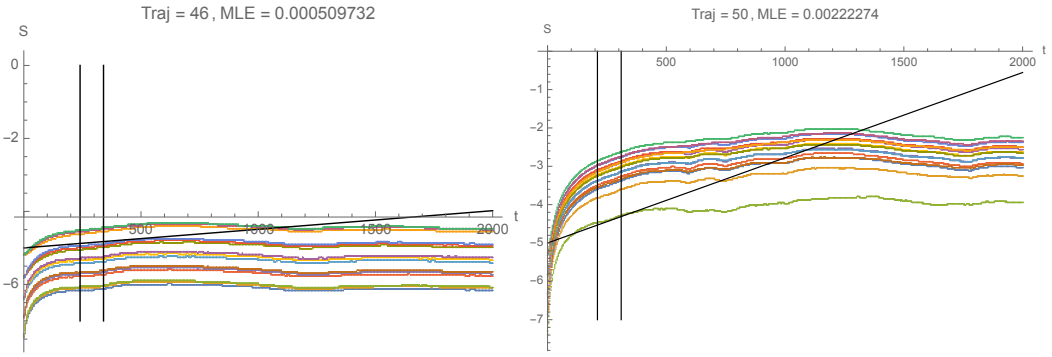

(a) $x_0 = 970.97$

(b) $x_0 = 1013.39$

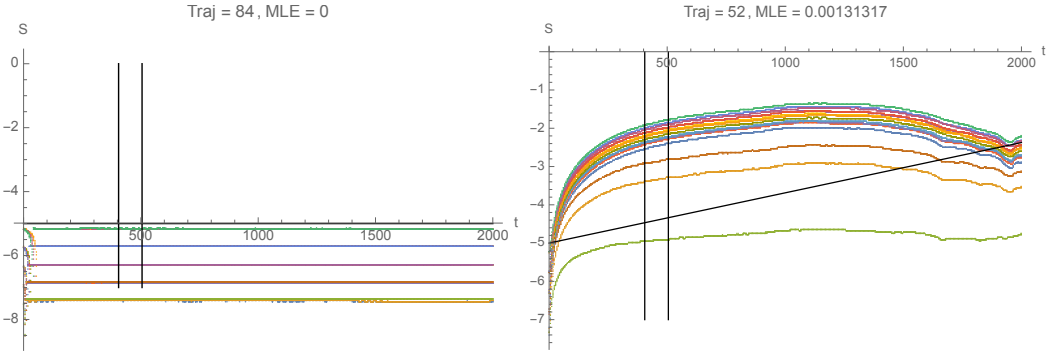

(c) $x_0 = 1374.02$

(d) $x_0 = 1034.61$

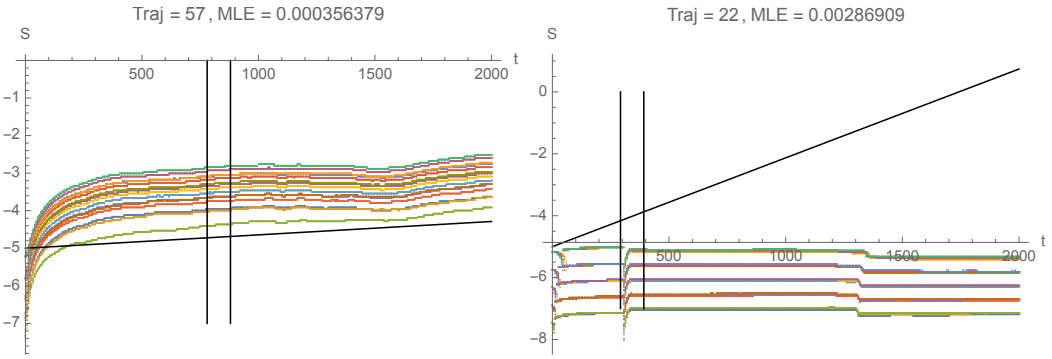

(e) $x_0 = 1087.64$

(f) $x_0 = 716.41$

Figure 5.12: Plots of $S(\tau)$ with the fitted line to measure the MLE and the range considered as the scaling region.

trajectory is found for many realisations and then averaged these anomalous results should have less impact, unless this is a recurring problem over many realisations. If so then it should be spotted as a spike in the data with an unusually large error bar from the standard error for the regression slope, and hence it can be ignored.

So overall, despite a few anomalous results, this program seems to be able to correctly identify the correct scaling region for the MLE estimation and it should be sufficient for finding the MLE for many trajectories, realisations and values of disorder.

Also shown by figures 5.13 and 5.14 are plots of MLE against the trajectory initial position, for disorder $w = 0.5, 1.0, 1.5, 2.0$. The error bars represent the value of the standard error of the regression slope.

Figures 5.13 and 5.14 show the output MLE against trajectory initial position for only one realisation. The curve oscillates rapidly for all four values of disorder, hence why an average over many realisations is required. An idea of the result for the averaged MLE over many more realisations could be discerned, with a sort of peak forming in the middle of the trajectory range for $w = 0.1$ which spreads as the value of disorder increases. Also, note the large error bars for trajectories 11 and 22 for $w = 0.5$ and trajectory 15 for $w = 1.0$, which shows that the fitted line was not very close to the $S(\tau)$ points. In fact, the trajectory 22 mentioned previously in figure 5.12f is the same trajectory as the one in 5.13a. So the error bars can be used to help determine at a glance whether the same situation occurs for a trajectory as for trajectory 22 mentioned previously. This helps to understand any strange oscillations that could occur for the average MLE against trajectory initial position plots.

So now the mean average MLE can be found for each trajectory, which can be used to create a plot of average MLE against trajectory initial position as shown in figures 5.15, 5.16 and 5.17.

The average MLE against trajectory initial position plots such as those of figure 5.15 do indeed show a more smooth result, and the strange oscillating points at the edges are potentially explained as a repeat of the situation from figure 5.12f as suggested by their larger error bars. There are also distinct peaks at the trajectory number ranges 35–55 for figure 5.15a and 35–65 for figure 5.15b, which seem to be of significance. As the disorder increases the width of these peaks increases as shown in figures 5.15, 5.16 and 5.17. This makes sense when comparing to figure 5.11, where for lower disorders the outer trajectories continue as though there is zero potential. Then for increasing disorder more outer trajectories start deviating from their usual path for zero potential, meaning their behaviour becomes chaotic.

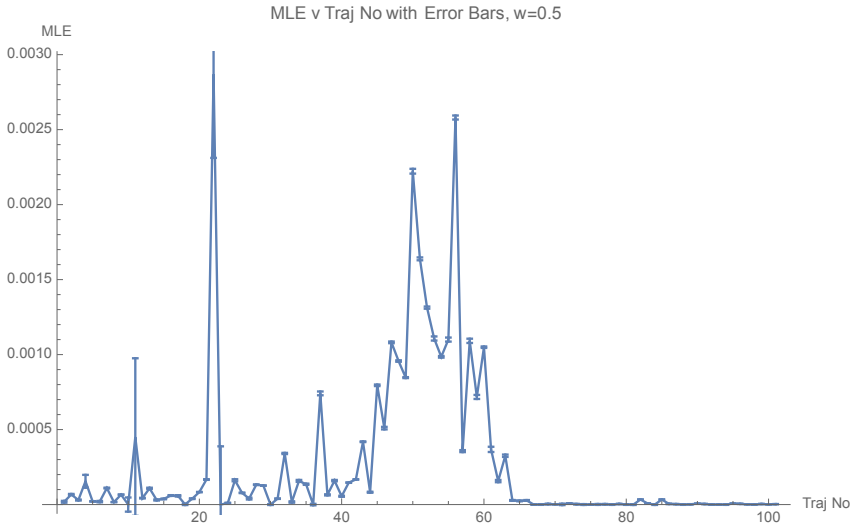

(a) $w = 0.5$

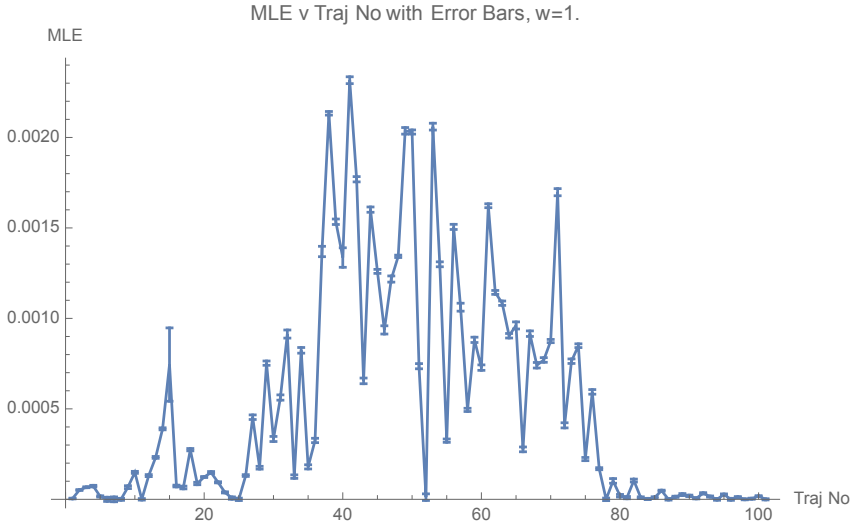

(b) $w = 1.0$

Figure 5.13: MLE is plotted against the trajectory initial position, with each trajectory equally spaced. Note that the error bars represent the value of the standard error of the regression slope.

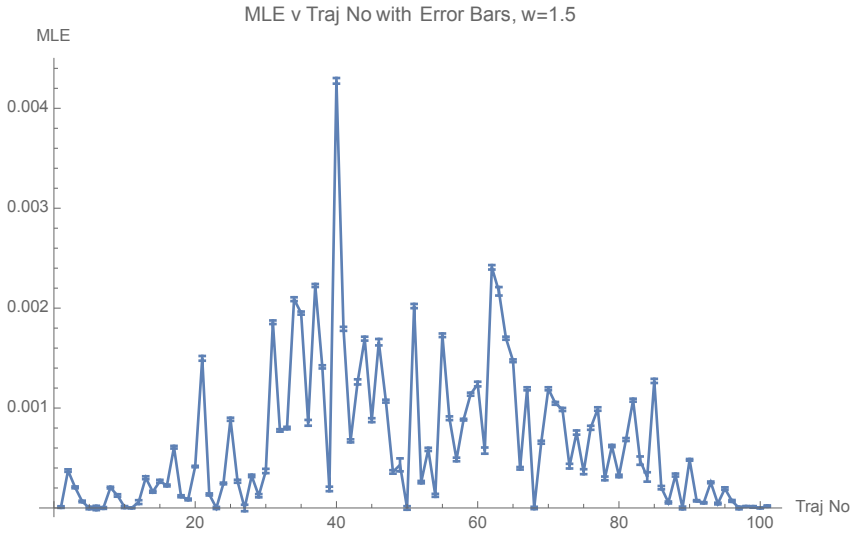

(a) $w = 1.5$

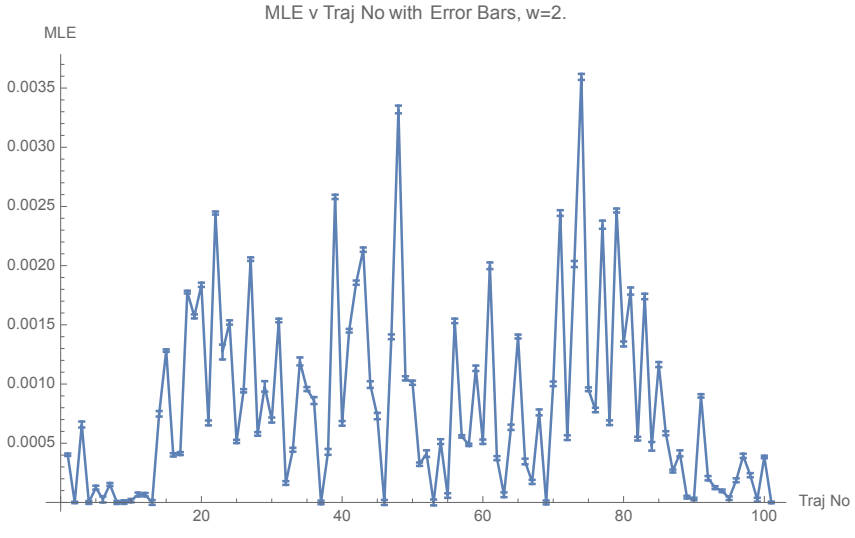

(b) $w = 2.0$

Figure 5.14: MLE is plotted against the trajectory initial position, with each trajectory equally spaced. Note that the error bars represent the value of the standard error of the regression slope.

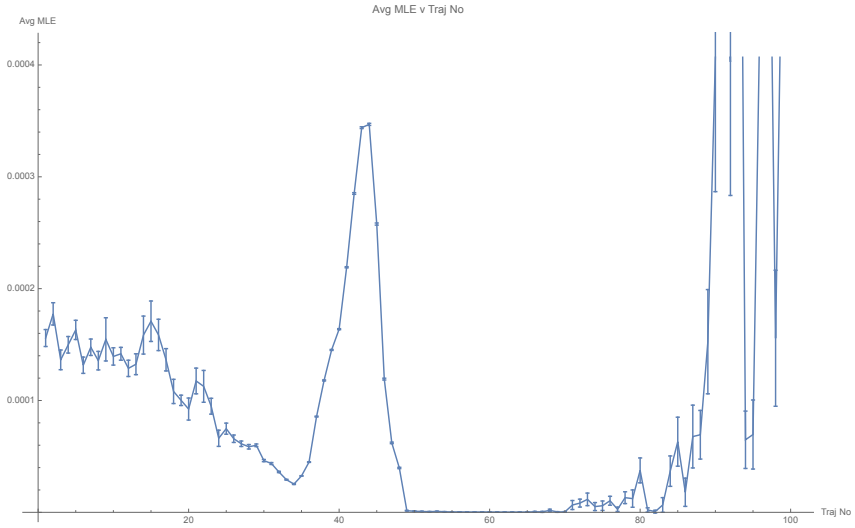

(a) $w = 0.1$

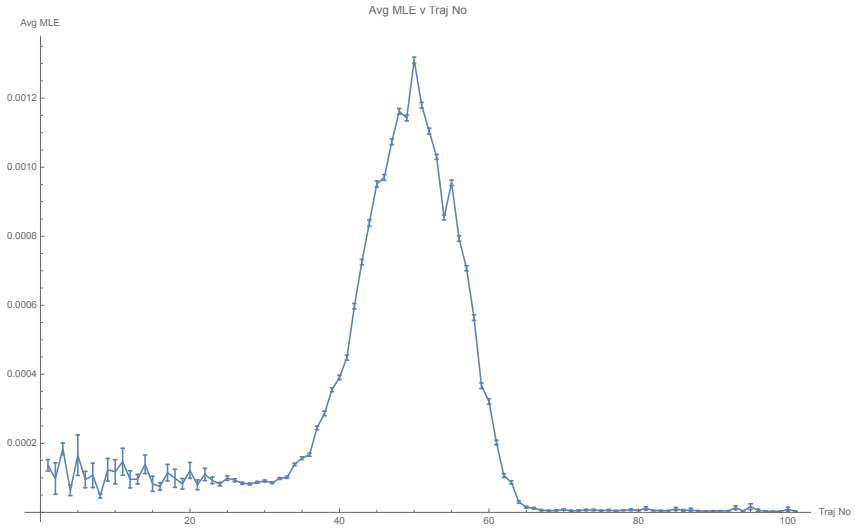

(b) $w = 0.5$

Figure 5.15: Plots of average MLE against trajectory initial position.

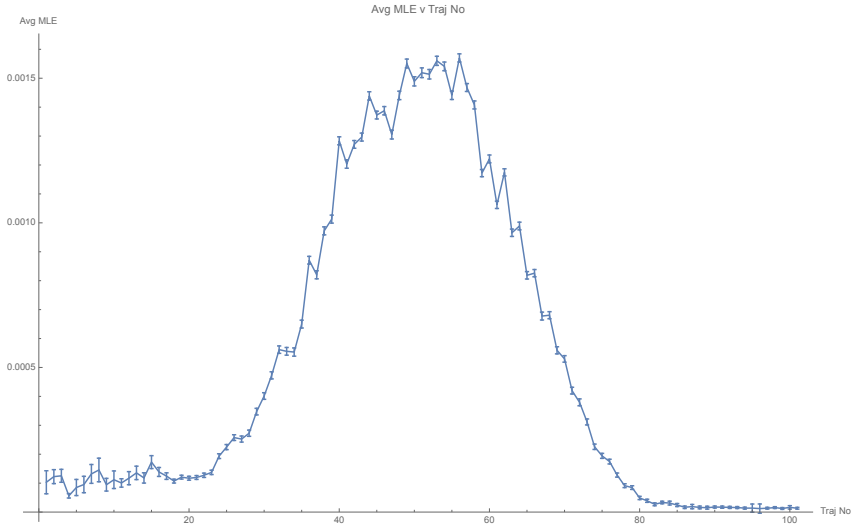

(a) $w = 1.0$

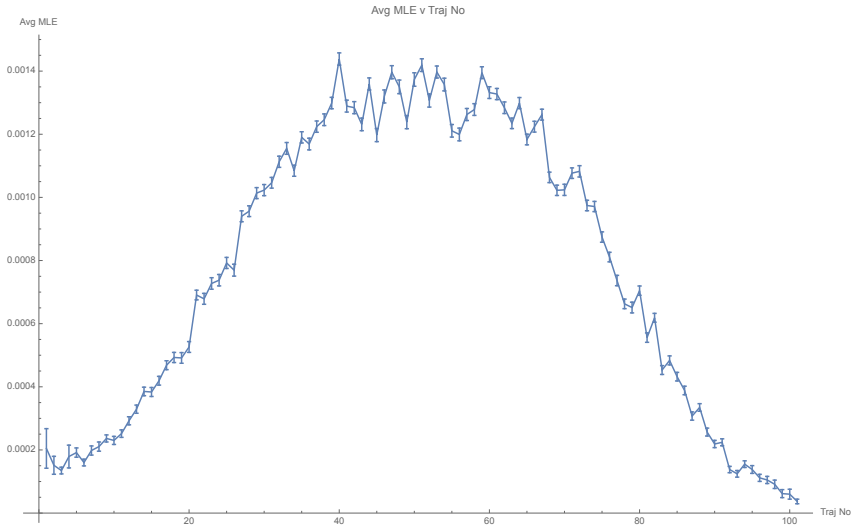

(b) $w = 1.5$

Figure 5.16: Plots of average MLE against trajectory initial position.

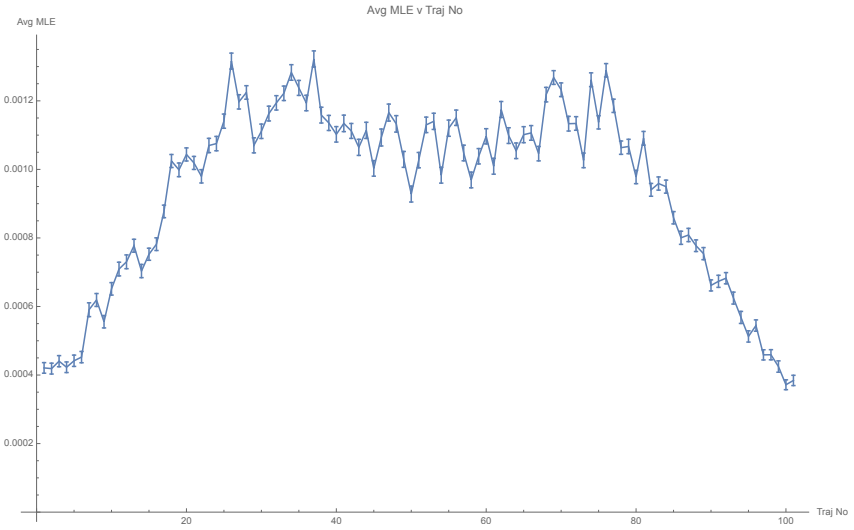

Figure 5.17: $w = 2.0$. Plot of average MLE against trajectory initial position.

Interestingly the peak appears to split in two when the disorder reaches $w = 2.0$, which could be explained by how trajectories tend to behave in the centre of the wave in the Anderson model. Again by referring to figure 5.11e it can be seen that the central trajectories stop moving in x-space very quickly and then remain stationary except for some small, seemingly random oscillating behaviour. The trajectories with larger MLEs could be those in a region transitioning from the trajectories travelling closer to their original velocity on the outside and those stationary in the middle. This could cause the trajectories in this region to oscillate slightly more unpredictably. Through this reasoning it is possible that the shape of the curve for disorder $w = 2.0$ could be occurring for all disorders, granted enough initial positions for trajectories were tried and provided the grid has enough grid points. The two peaks could simply be too small to see in the plots provided. It would also be interesting to observe the behaviour of the peaks splitting for larger disorders, or other disorders between $w = 1.5$ and $w = 2.0$.

Gaussian curves can be fitted to these average MLE against trajectory initial position plots, with the results shown in figures 5.18, 5.19 and 5.20. Table 5.1 shows the parameters of the fitted Gaussian curves for each value of disorder.

The fitted Gaussian curves shown in figures 5.18, 5.19 and 5.20 can be used to help analyse the observed peaks in the average MLE against trajectory initial position plots. With the exception of disorder $w = 2.0$, which has a double peak, the fitted Gaussian curves match the plots reasonably well. Table 5.1 shows the rms width increasing as the value of disorder increases, as expected from looking at the

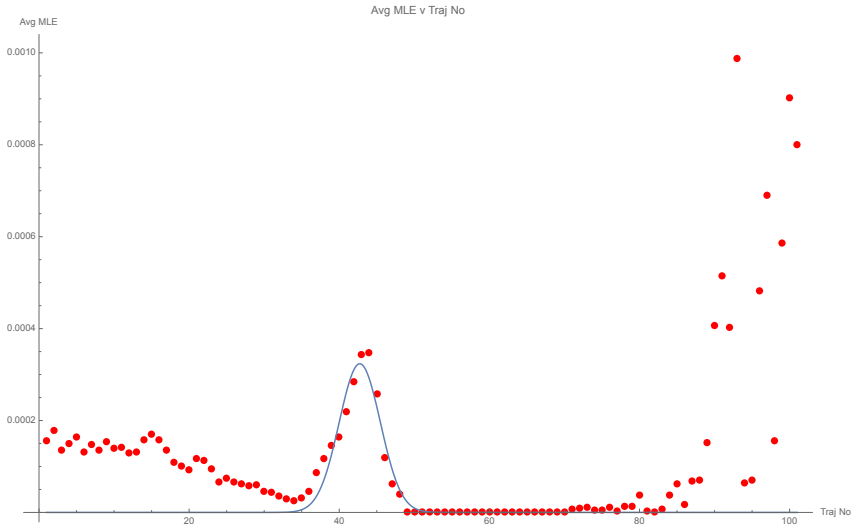

(a) $w = 0.1$

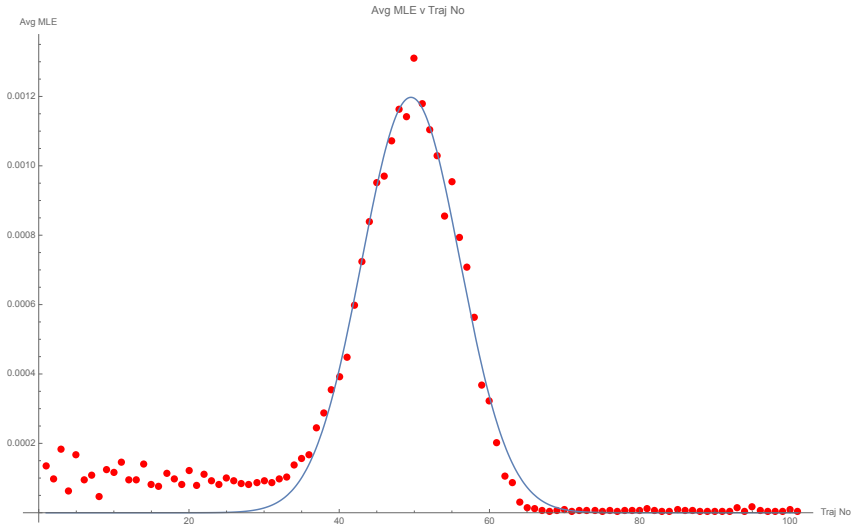

(b) $w = 0.5$

Figure 5.18: Average MLE against trajectory initial position plots with fitted Gaussian curves.

Disorder	Height	Position of Centre	Width
0.1	0.0003235	42.74	2.741
0.5	0.001197	49.55	6.543
1.0	0.001557	50.77	12.78
1.5	0.001420	50.47	22.78
2.0	0.001216	50.50	38.64

Table 5.1: Table showing the parameters of the fitted Gaussian curves for each disorder.

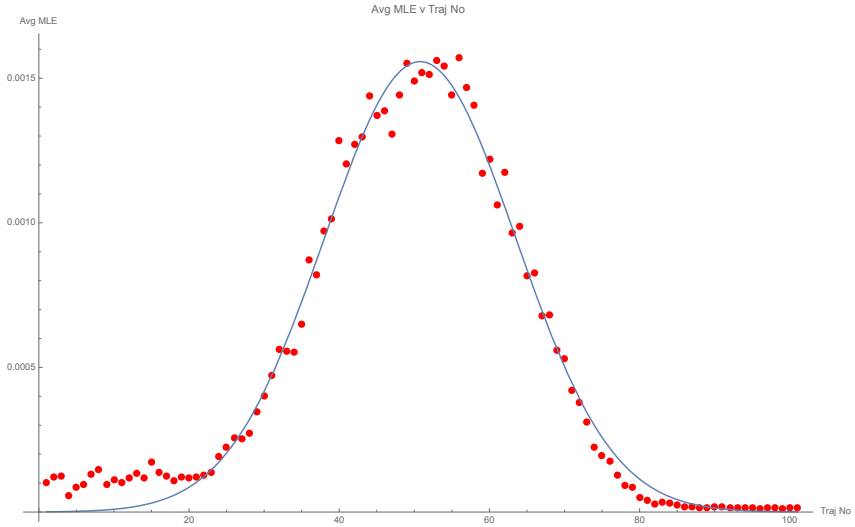

(a) $w = 1.0$

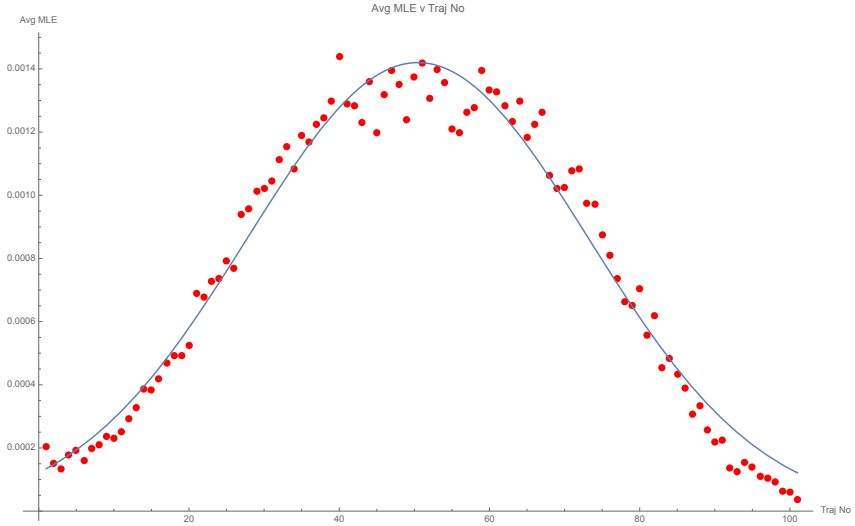

(b) $w = 1.5$

Figure 5.19: Average MLE against trajectory initial position plots with fitted Gaussian curves.

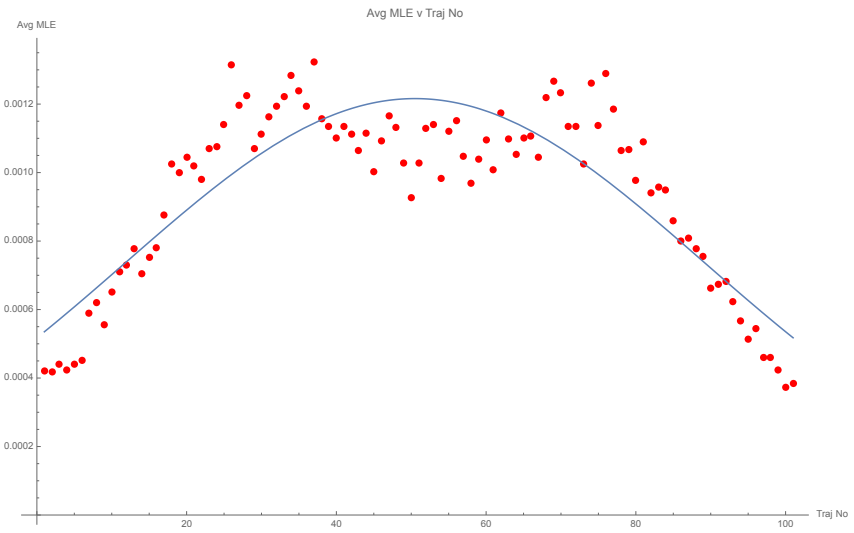

Figure 5.20: $w = 2.0$. Average MLE against trajectory initial position plots with fitted Gaussian curves.

plots. This shows that the number of chaotic trajectories increases as the disorder increases. The height of the Gaussian curves quickly increases to about 0.0015 and then decreases after that steadily, so the largest MLE for any trajectory is of the order 10^{-3}. This shows that how chaotic the trajectory can be, in other words the maximum MLE obtainable, stays at the same level after a certain value of disorder and only the number of chaotic trajectories increases. The position of the centre of the Gaussian curve also increases, always being close to the centre of the grid and getting closer to the centre for larger values of disorder. Note that it never quite reaches the centre of the grid, at trajectory number 51. What this suggests is that the trajectories are slightly more chaotic below the centre of the grid. This is explained by the non-zero initial velocity, and can be seen by considering figure 5.11. For any non-zero value of disorder the trajectories with a smaller initial position change direction and move in the opposite direction. This change in direction could be counting towards the MLE calculation, making the trajectory more chaotic. So the off-centre values of the position of the Gaussian curves can be explained as simply a side effect of the initial velocity of the trajectories.

Additionally a plot of rms width against disorder is shown in figure 5.21 along with a fitted quadratic curve.

Figure 5.21 indicates a possible quadratic relation between the rms width of the fitted Gaussian and the value of disorder. This means that by analysing the MLEs of trajectories in the Anderson model the localization length could be found using the Thouless Formulae (see equation (2.26), for the centre of the band energy).

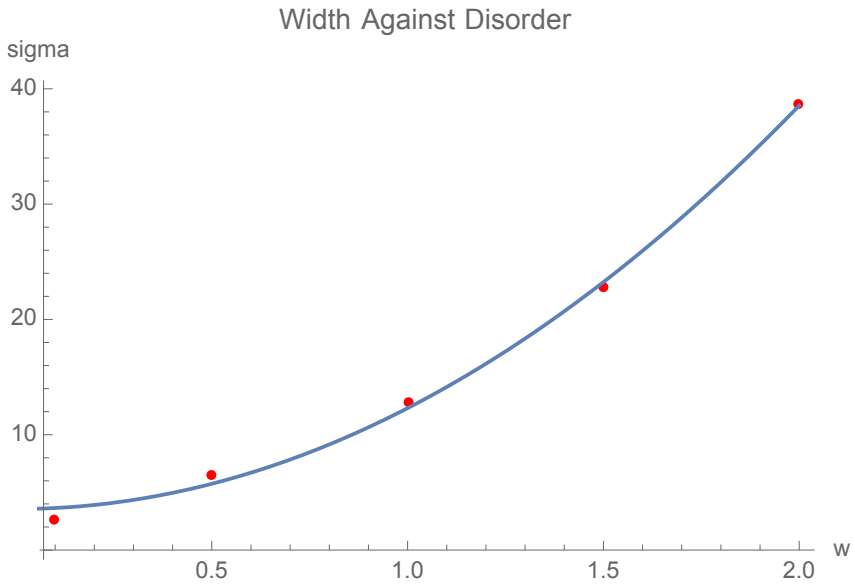

Figure 5.21: Plot of rms width of fitted Gaussian against disorder (red), and a fitted quadratic curve (blue).

Finally for different realisations of each disorder w, controlled by the seed used to randomly generate the potential, the MLE for each trajectory in a given run of the simulation can be found and used for further analysis. For a given trajectory the distribution of MLEs can be found, with the distributions for the central trajectory using different values of disorder given by figure 5.22.

While the average MLE against trajectory initial position is useful for looking at the overall dynamics of the ensemble of trajectories, to look at each trajectory individually the histograms of MLEs for each trajectory could be used, like the ones shown in figure 5.22. In this example, the central trajectory is used so one would expect the average MLE to generally increase until the peaks split and the MLE dips. Figure 5.22a shows that the MLE can be considered to be zero for $w = 0.1$ in comparison with the MLE for larger values of disorder. The distribution for the central trajectory seems to get more spread out as the value of disorder increases, again with the exception of $w = 2.0$. Additionally, there appears in every plot a small secondary peak at a slightly larger value of disorder. Without a numerical analysis it is difficult to draw any conclusions relating to the Anderson model with these histograms, but it is evidently possible due to the features described here.

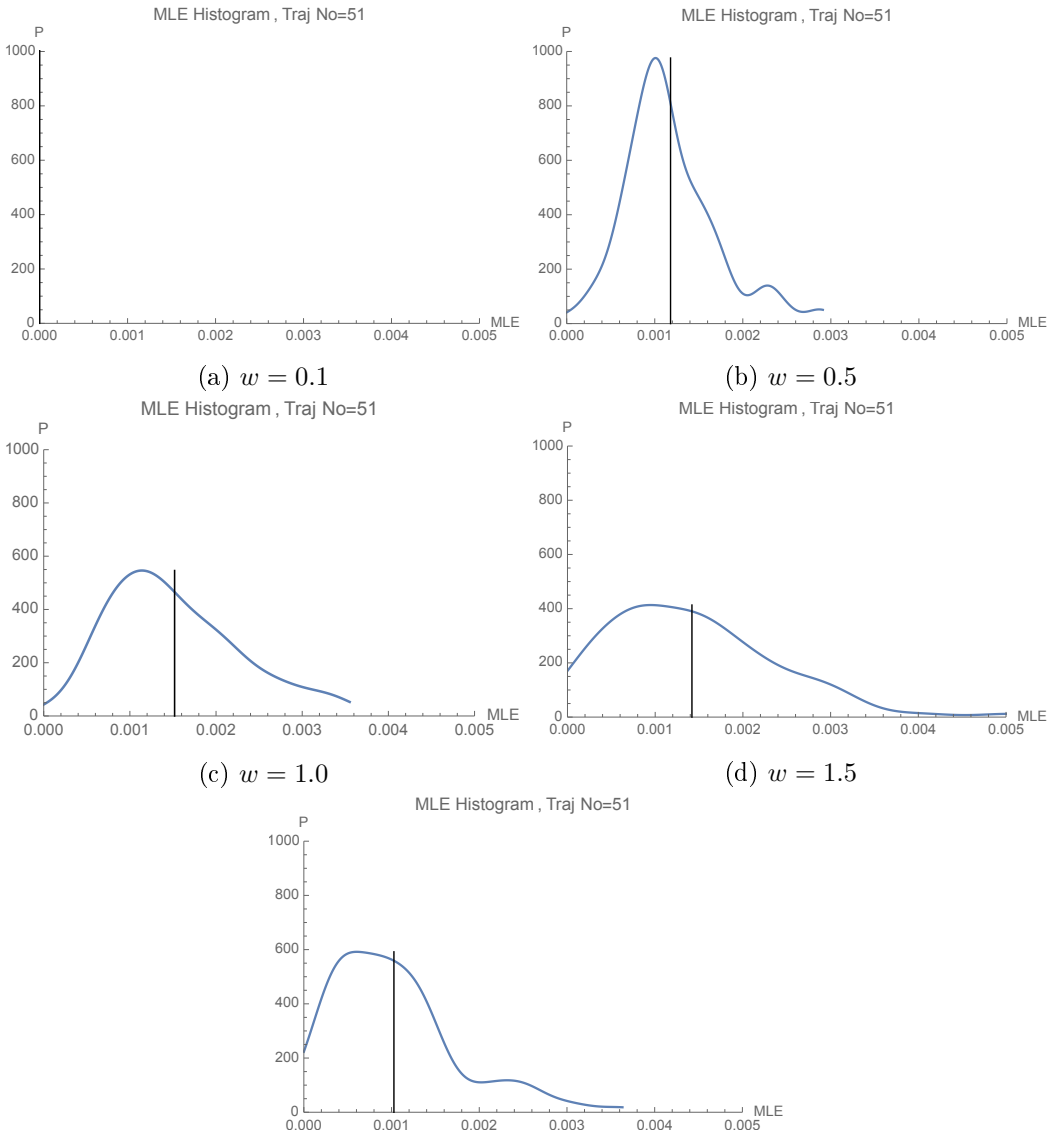

(a) $w = 0.1$

(b) $w = 0.5$

(c) $w = 1.0$

(d) $w = 1.5$

(e) $w = 2.0$

Figure 5.22: Distributions of MLEs found for the central trajectory, for different values of disorder. The vertical line represents the average MLE.

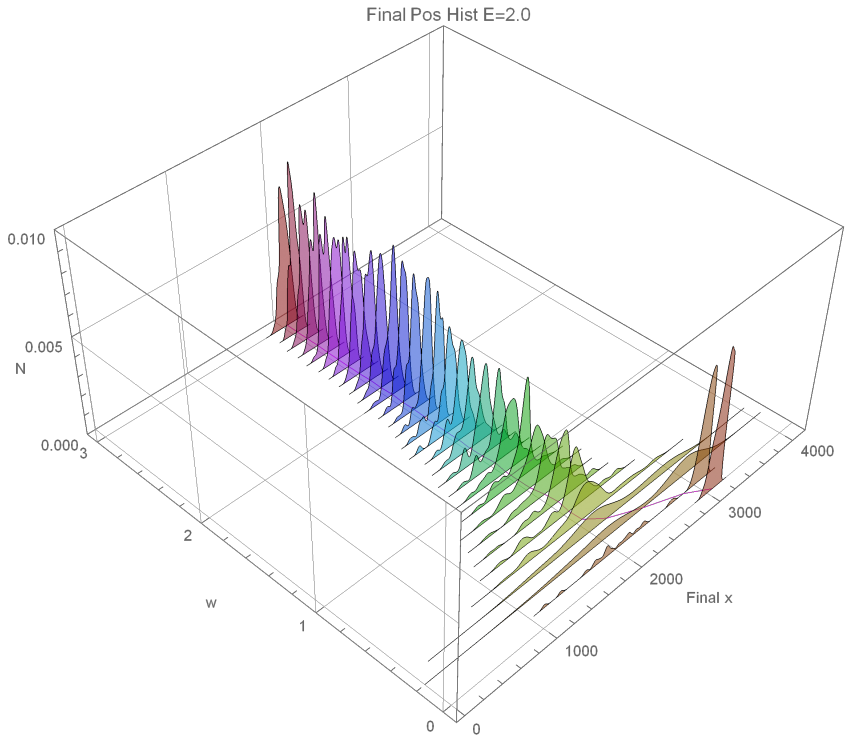

Figure 5.23: The histograms of final positions for 101 trajectories is shown for each disorder $w = 0.0, ..., 3.0$. The blue line represents the mean average of positions for each histogram.

5.2.2 Position and Velocity Distributions

The three-dimensional plots shown in this subsection represent stacked two-dimensional smooth histograms, with each histogram representing different values of disorder w.

Figure 5.23 shows histograms of the positions of trajectories for each disorder at the final time step. Trajectories are initialised according to the Born rule, and the number of x-points totals 4096 with the number of time steps being 12288. By setting random positions (equal to the number of trajectories used) within the grid range according to the Born rule, smooth histograms can be plotted as shown by figure 5.24 which effectively gives a smoothed over plot for the amplitude of the wave function at each x-position for the final time step. This can be compared to the final position histograms. Finally, the difference plots for the trajectory final position histograms and the Born rule histograms is shown by figure 5.25.

Figure 5.23 shows what behaviour could be expected of particles when the wave function is in the localized or diffusive state. For high values of disorder the final position of particles is within a fixed range, when the system is in a localized state. For small values of disorder the particles travel roughly parallel to each other

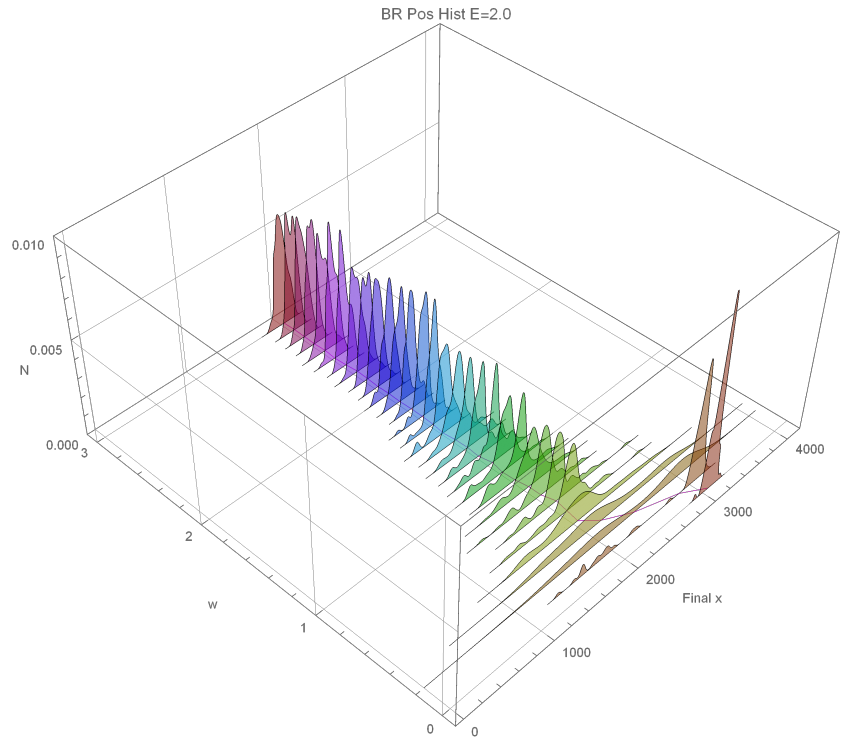

Figure 5.24: The histograms of 101 positions set randomly according to the Born rule at the final time step, for disorder $w = 0.0, ..., 3.0$. The blue line represents the mean average of positions for each histogram.

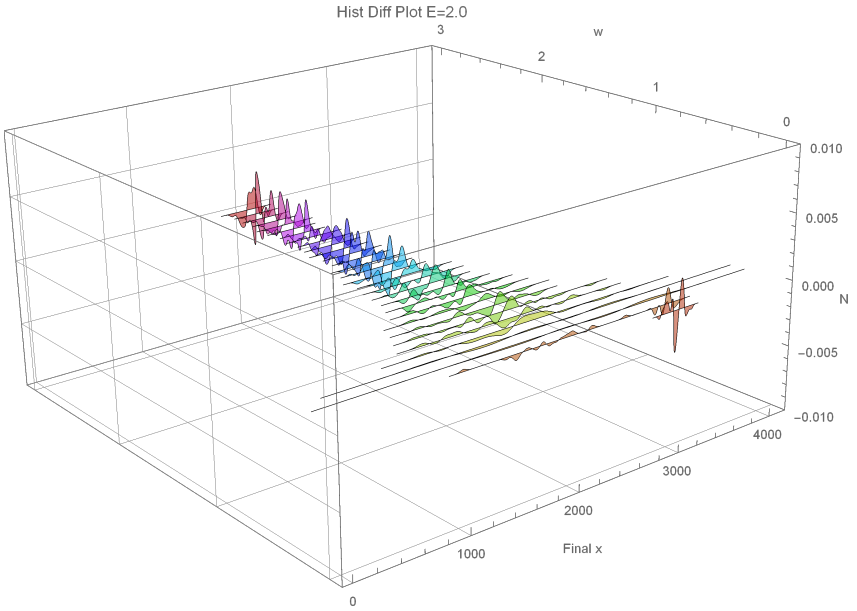

(a) Side-view

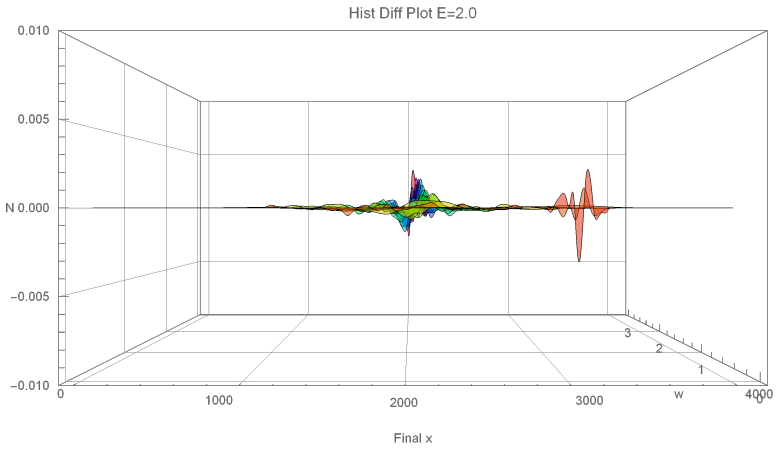

(b) Head-on

Figure 5.25: Series of difference plots between trajectory final position histograms and Born rule histograms.

in straight lines, at approximately their initial velocity, so the particles stay within the same distance from each another which produces the peak at their final position. Between the localized and diffusive states the particles appear to be more spread in their final position. This is a cross-over between the diffusive and localized states, where the peak in the histograms goes from wherever the final position of the wave is for zero potential to the peak at the initial position of the wave. The blue line representing the mean position for each histogram can be used to help see this, with the line initially at the final position of the wave for zero disorder converging towards the centre of the grid, when the wave is localized.

It could be considered by looking at figure 5.23 that $w = 0.0, 0.1$ are both in the diffusive phase, $w = 0.2, 0.3$ are both in the cross-over phase and values of disorder at $w = 0.4$ and above are in the localized state. The values of disorder observed for chaotic behaviour were $w = 0.1, 0.5, 1.0, 1.5, 2.0$ (see subsection 5.2.1), meaning that the cross-over phase may not have been considered for analysis which is something which could be done in future. It also shows that there is less chaotic behaviour for systems in the diffusive state compared to the localized state.

Additionally, figure 5.23 can be used to show that the Born rule remains consistent throughout the simulation and therefore that the trajectory propagation is accurate. This is simple due to how the trajectories here are initialised according to the Born rule, so the histograms just need to be compared to the square of the amplitude of the wave function. To create a smooth plot a histogram of positions initialised at the final time step is created and this is shown in figure 5.24, which can be directly compared to figure 5.23. A difference plot shown in figure 5.25 between each pair of histograms shows that the difference is relatively small for each value of disorder and therefore that the trajectories are still distributed according to the Born rule as they were initially. The difference is likely to originate from there only being 101 trajectories for a grid size of 4096. So the Born rule holds according to the distribution of trajectories, so the trajectories appear to be propagating correctly. This conclusion is also supported by the blue line representing the mean position for each histogram, with the line looking close to identical between the final position histograms and the histograms of positions initialised at the final time step.

Shown in figures 5.26 and 5.27 are a series of smooth histograms involving the average velocity over the entire simulation time for each trajectory and also over the final 2000 time steps. Here the trajectories are again initialised according to the Born rule and the number of time steps equal 12288, but the grid contains 2048 points. The initial velocity for all particles is $v_0 = 2$.

The average velocity over time histograms can also be compared to the lo-

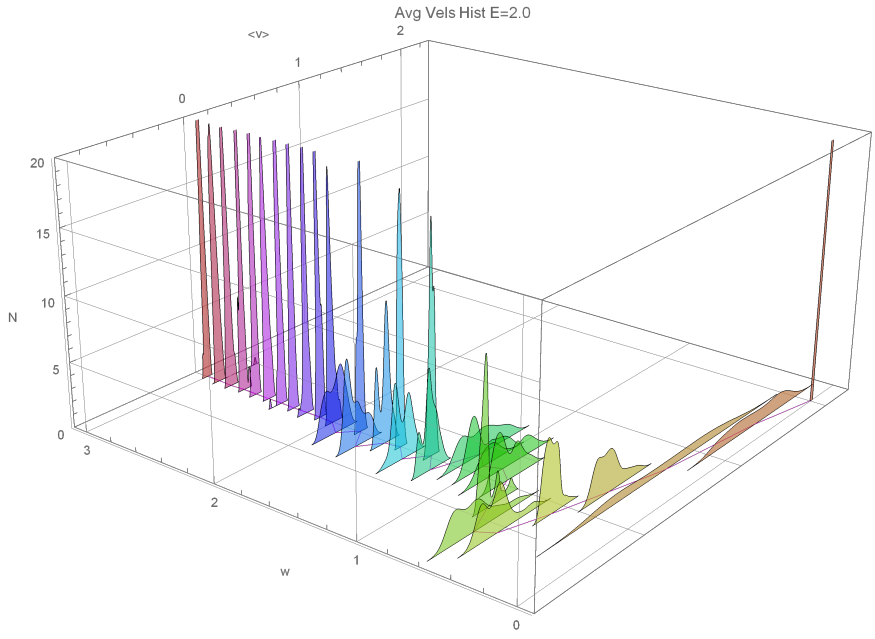

Figure 5.26: A series of histograms for the average velocity over time for each individual trajectory, with each histogram representing a different value of disorder. The blue line shows the mean average of the average velocities for each histogram.

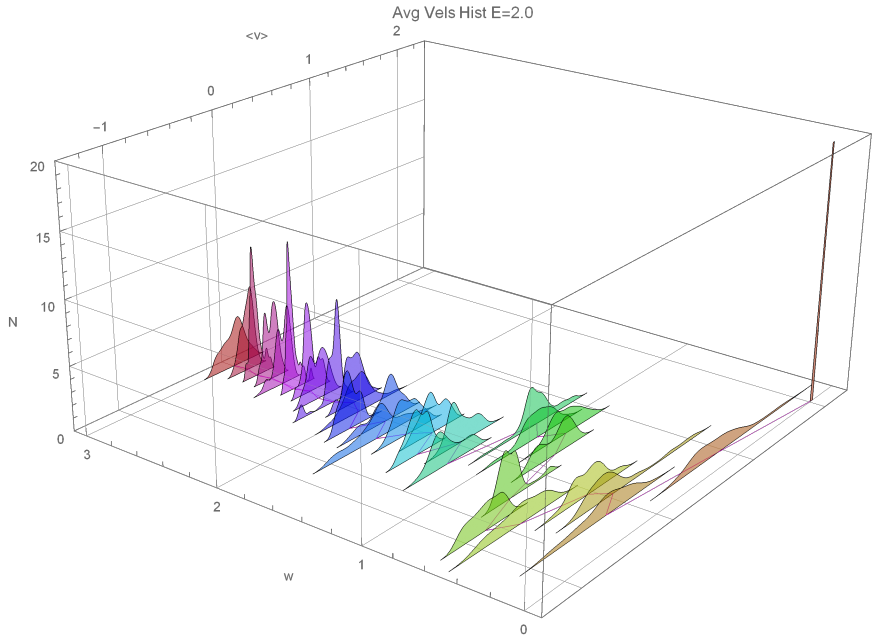

Figure 5.27: The same as for figure 5.26 but now the average is only over the final 2000 time steps.

calized and diffusive phases of the wave function. Any peak at the initial velocity for low disorder shows the diffusive phase, the peaks at zero velocity represent the localized phase and the peaks in-between show systems in the cross-over phase. The average velocity over all time steps histograms, shown in figure 5.26, shows more distinct peaks than the average velocity over the last 2000 time steps histograms, shown in figure 5.27. This is simply due to the larger sample size for the averaging for figure 5.26. However, figure 5.27 may show more accurately the direction a given trajectory ultimately travels in. The relative similarity between the two figures shows that most trajectories travel in a general direction for the majority of the simulation time.

These average velocity over time histograms show the expected result, since localized trajectories would not be expected to travel anywhere. If they did then they would enter regions where the wave amplitude is low and therefore the particle is unlikely to be there, and since trajectories cannot cross a lot of trajectories would end up in that region. The case of low disorder is close to a zero potential system, meaning trajectories end up travelling close to their initial velocity.

Looking at figure 5.26 the interesting case is the cross-over phase, with the average velocities having a large spread of values at $w = 0.2$ before the distribution becomes more peaked at $w = 0.3$ at a value relatively close to zero. After that the mean value of the average velocities, represented by the blue line, shows that the trajectories oscillate in velocity and then converge towards zero velocity. The oscillation in velocity described here in an interesting effect that is difficult to explain and would need to be studied further.

Chapter 6

Conclusions

The simulation is accurate on the evidence given, with the wave propagation methods producing results matching the analytical solution for a free wave. The boundaries work well enough for a large grid size, though it is difficult to eliminate unwanted reflections and transmissions of the wave for absorbing boundaries without adding too much extra computation. Even though the amplitude is mostly eliminated, the small part of the wave that still exists alters the phase and therefore the trajectories. The trajectory evolution also follows predicted paths correctly for the zero potential system. So overall the simulation works for the zero potential case and hence if a potential is added correctly the simulation should also produce the correct results for systems with a non-zero potential. The resulting trajectories can be plotted for their position at their current time in order to visualise the Bohm particle motion, and get an idea for the behaviour of the system for various initial positions of the particles.

The calculation of the MLEs using TISEAN appears to work correctly, as does the program to identify the scaling region on the $S(\tau)$ plots for most cases. Therefore it is possible to calculate the MLEs for many trajectories in a simulation, over many realisations of the system for each given disorder in a reasonable amount of time. The results from calculating these MLEs can be analysed, with sensible distributions of MLEs per trajectory. In future these distributions could be analysed more quantitatively so that the dynamics of the individual trajectories can be described. The overall chaotic behaviour of the ensemble of trajectories shows trends which can understood; after plotting the average MLE against trajectory initial position Gaussian curves can be fitted so that the width of the peaks can be measured. The resulting rms widths measured show a possible quadratic relation for the rms width as a function of disorder, though more results would be needed

to confirm this. If true then a relation between the rms width and the localization length can be found using the Thouless formulae, meaning that properties of the system that can be observed can be found using only the behaviour of trajectories in de Broglie-Bohm theory.

The position and velocity histograms for the trajectories could be used to identify what state the system is in, though their uses in studying individual trajectories is limited. This is because a lot of the information about the behaviour of each trajectory is lost, especially in the position histograms, and so it should only be useful for analysing the ensemble of trajectories. In future a more quantitative analysis of these histograms could be performed which could provide more information about the system.

The process for studying trajectories in the Anderson model could be to use the position or velocity histograms to identify the values of disorder for which the system is in a localized or diffusive state. Then the analysis of the MLEs over many realisations can be conducted in order to measure how chaotic the system is in each state or value of disorder. Effects that are easily observed could be studied using the average MLE against trajectory initial position plots. By analysing the MLE distributions for specific trajectories effects that are difficult to observe could be found, allowing for a more microscopic view of the system than possible with ordinary quantum theory, as initially intended by Bohm. Therefore de Broglie-Bohm theory could be used to study Anderson localization, though it is too inefficient for studying these systems as a whole so its uses in research would be for studying the system on a smaller scale. Beyond Anderson localization in one dimension, it would be instructive to study the three-dimensional Anderson model in this way. Then research on the critical phase of the wave function in de Broglie Bohm theory can be conducted. Additionally, de Broglie Bohm theory can be used in the same way on the Aubry-André model.

Appendices

Appendix A

Standard Error of the Regression Slope

The standard error of the regression slope is given by

$$S_{err} = \frac{\sqrt{\sigma^2}}{\sqrt{\sum_i (x_i - \bar{x})^2}}, \tag{A.1}$$

with x_i being the values from the data points, $\bar{x}$ being the average of the x data values and the variance calculated using

$$\sigma^2 = \frac{\sum_i (y_i - \hat{y}_i)^2}{n - p}. \tag{A.2}$$

Here $y_i - \hat{y}_i$ is the ith residual, the difference between the y-value of the data point and the y-value of the line. n represents the number of data points and p represents the number of parameters in the model, which is two in this context.

The standard error of the regression slope shows how the average distance of the observed values deviate from the regression line, so it can be used to measure how good the fitted line is for the given data (Teague [2007], Andale [2013], Wolfram [2008]). The variance for each line in a $S(\tau)$ plot is calculated using equation (A.2), then the average variance is used in equation (A.1). This calculated standard error for the regression slope is used for the error bars in the MLE against trajectory initial position plots, for a given realisation and disorder w. For the error bars in the average MLE against trajectory initial position plots, the average standard error of the regression slope is used.

Bibliography

E. Abrahams, P. W. Anderson, D. C. Licciardello, and T. V. Ramakrishnan. Scaling theory of localization: Absence of quantum diffusion in two dimensions. *Phys. Rev. Lett.*, 42:673–676, Mar 1979. doi: 10.1103/PhysRevLett.42.673. URL https://link.aps.org/doi/10.1103/PhysRevLett.42.673.

Anthony Aguirre and Max Tegmark. Born in an infinite universe: A cosmological interpretation of quantum mechanics. *Phys. Rev. D*, 84:105002, Nov 2011. doi: 10.1103/PhysRevD.84.105002. URL https://link.aps.org/doi/10.1103/PhysRevD.84.105002.

Andale. Standard Error of Regression Slope. http://www.statisticshowto.com/find-standard-error-regression-slope/, 2013. Accessed: 2017-10-23.

P. W. Anderson. Absence of diffusion in certain random lattices. *Phys. Rev.*, 109:1492–1505, Mar 1958. doi: 10.1103/PhysRev.109.1492. URL http://link.aps.org/doi/10.1103/PhysRev.109.1492.

David Bohm. A suggested interpretation of the quantum theory in terms of "hidden" variables. i. *Phys. Rev.*, 85:166–179, Jan 1952a. doi: 10.1103/PhysRev.85.166. URL https://link.aps.org/doi/10.1103/PhysRev.85.166.

David Bohm. A suggested interpretation of the quantum theory in terms of "hidden" variables. ii. *Phys. Rev.*, 85:180–193, Jan 1952b. doi: 10.1103/PhysRev.85.180. URL https://link.aps.org/doi/10.1103/PhysRev.85.180.

F Borondo, A Luque, J Villanueva, and D A Wisniacki. A dynamical systems approach to bohmian trajectories in a 2d harmonic oscillator. *Journal of Physics A: Mathematical and Theoretical*, 42(49):495103, 2009. URL http://stacks.iop.org/1751-8121/42/i=49/a=495103.

T. Brandes and S. Kettemann. *Anderson Localization and Its Ramifications: Disorder, Phase Coherence, and Electron Correlations*. Lecture Notes in Physics. Springer Berlin Heidelberg, 2003. ISBN 9783540407850. URL https://books.google.co.uk/books?id=EaFjyalWGFMC.

J. G. Cramer. The Transactional Interpretation of Quantum Mechanics and Quantum Nonlocality. *ArXiv e-prints*, February 2015.

O. F. de Alcantara Bonfim, J. Florencio, and F. C. Sá Barreto. Quantum chaos in a double square well: An approach based on bohm's view of quantum mechanics. *Phys. Rev. E*, 58:6851–6854, Nov 1998. doi: 10.1103/PhysRevE.58.6851. URL https://link.aps.org/doi/10.1103/PhysRevE.58.6851.

H. Everett. *Theory of the Universal Wavefunction*. PhD thesis, 1956.

Hans Frisk. Properties of the trajectories in bohmian mechanics. *Physics Letters A*, 227(3):139 – 142, 1997. ISSN 0375-9601. doi: https://doi.org/10.1016/S0375-9601(97)00044-3. URL http://www.sciencedirect.com/science/article/pii/S0375960197000443.

Murray Gell Mann and James B. Hartle. Decoherent histories quantum mechanics with one 'real' fine-grained history. 85, 06 2011.

L. Hardy and R. Spekkens. Why Physics Needs Quantum Foundations. *ArXiv e-prints*, March 2010.

R. Hegger, H. Kantz, and T. Schreiber. Practical implementation of nonlinear time series methods: The TISEAN package. *CHAOS*, 9, 1999.

P.R. Holland. *The Quantum Theory of Motion: An Account of the de Broglie-Bohm Causal Interpretation of Quantum Mechanics*. Cambridge University Press, 1995. ISBN 9780521485432. URL https://books.google.co.uk/books?id=BsEfVBzToRMC.

Guglielmo Iacomelli and Marco Pettini. Regular and chaotic quantum motions. *Physics Letters A*, 212(1):29 – 38, 1996. ISSN 0375-9601. doi: https://doi.org/10.1016/0375-9601(96)00027-8. URL http://www.sciencedirect.com/science/article/pii/0375960196000278.

H. Kantz. A robust method to estimate the maximal Lyapunov exponent of a time series. *Physics Letters A*, 185:77–87, January 1994. doi: 10.1016/0375-9601(94)90991-1.

R. Kosloff and D. Kosloff. Absorbing boundaries for wave propagation problems. *Journal of Computational Physics*, 63(2):363 – 376, 1986. ISSN 0021-9991. doi: http://dx.doi.org/10.1016/0021-9991(86)90199-3. URL http://www.sciencedirect.com/science/article/pii/0021999186901993.

F M. Izrailev, A A. Krokhin, and N M. Makarov. Anomalous localization in low-dimensional systems with correlated disorder. 512, 10 2011.

R.H. Parmenter and R.W. Valentine. Deterministic chaos and the causal interpretation of quantum mechanics. *Physics Letters A*, 201(1):1 – 8, 1995. ISSN 0375-9601. doi: https://doi.org/10.1016/0375-9601(95)00190-E. URL http://www.sciencedirect.com/science/article/pii/037596019500190E.

Gerald Schubert and Holger Fehske. Dynamical aspects of two-dimensional quantum percolation. *Phys. Rev. B*, 77: 245130, Jun 2008. doi: 10.1103/PhysRevB.77.245130. URL http://link.aps.org/doi/10.1103/PhysRevB.77.245130.

J.C. Sprott. Henon Map Maximum Lyapunov Exponent and Kaplan-Yorke Dimension. http://sprott.physics.wisc.edu/chaos/henondky.htm, 2007. Accessed: 2017-10-17.

S.H. Strogatz. *Nonlinear Dynamics And Chaos*. Studies in nonlinearity. Sarat Book House, 2007. ISBN 9788187169857. URL https://books.google.co.uk/books?id=PHmED2xxrE8C.

D. Teague. Standard Errors for Regression. http://courses.ncssm.edu/math/Talks/, 2007. Accessed: 2017-10-23.

M. D. Towler, N. J. Russell, and Antony Valentini. Time scales for dynamical relaxation to the born rule. *Proceedings of the Royal Society of London A: Mathematical, Physical and Engineering Sciences*, 468(2140): 990–1013, 2012. ISSN 1364-5021. doi: 10.1098/rspa.2011.0598. URL http://rspa.royalsocietypublishing.org/content/468/2140/990.

R. Uppu. An Introduction to Hamilton-Jacobi Theory. http://www.cmi.ac.in/ ravitej/talk2.pdf, 2007. Accessed: 2017-12-17.

A. Valentini and H. Westman. Dynamical origin of quantum probabilities. *Proceedings of the Royal Society of London Series A*, 461:253–272, January 2005. doi: 10.1098/rspa.2004.1394.

A. Vulpiani. *Chaos: From Simple Models to Complex Systems*. Series on advances in statistical mechanics. World Scientific, 2010. ISBN 9789814277662. URL https://books.google.co.uk/books?id=_TuaDQAAQBAJ.

Wolfram. VarianceEstimatorFunction. http://reference.wolfram.com/language/ref/VarianceEstimatorFunction.html, 2008. Accessed: 2017-10-23.

Ciann-Dong Yang and Chia-Hung Wei. Strong chaos in one-dimensional quantum system. *Chaos, Solitons and Fractals*, 37(4):988 – 1001, 2008. ISSN 0960-0779. doi: https://doi.org/10.1016/j.chaos.2008.01.017. URL http://www.sciencedirect.com/science/article/pii/S0960077908000088.

W. H. Zurek. Quantum Darwinism. *Nature Physics*, 5:181–188, March 2009. doi: 10.1038/nphys1202.